PB-207 755

VENT AND STATION TEST (VST) FACILITY. VENT SHAFT TESTING

Developmental Sciences, Incorporated
City of Industry, California

August 1971

Distributed . . . 'to foster, serve and promote the nation's economic development and technological advancement.'

NATIONAL TECHNICAL INFORMATION SERVICE

U.S. DEPARTMENT OF COMMERCE

Technical Report No. UMTA-DC-MTD-7-71-21

PB 207 755

Institute for Rapid Transit
Washington, D.C.

VENT AND STATION TEST (VST) FACILITY — VENT SHAFT TESTING

August 1971

Prepared by
AEROSPACE TECHNOLOGY
Division of
DEVELOPMENTAL SCIENCES, INC.
City of Industry, California

for

UNITED STATES DEPARTMENT OF TRANSPORTATION
Urban Mass Transportation Administration
Washington, D.C. 20590

BIBLIOGRAPHIC DATA SHEET	1. Report No. UMTA-DC-MTD-7-71-21	2.	3. Recipient's Accession No.
4. Title and Subtitle VENT AND STATION TEST (VST) FACILITY - VENT SHAFT TESTING			5. Report Date August 1971
			6.
7. Author(s)			8. Performing Organization Rep. No.
9. Performing Organization Name and Address Aerospace Technology Division, Developmental Sciences, Inc., City of Industry, California			10. Project/Task/Work Unit No. DC-MTD-7
			11. Contract/Grant No. DOT-UT-290
12. Sponsoring Organization Name and Address Urban Mass Transportation Administration, 400 7th Street, S.W., Washington, D.C. 20590			13. Type of Report & Period Covered Milestone
			14.
15. Supplementary Notes Prepared for the Institute for Rapid Transit, Washington, D.C. 20006			

16. Abstracts

This report has been prepared under the Institute for Rapid Transit (IRT) project, "Ventilation and Environmental Control in Subway Rapid Transit Systems," ~~and is~~ one of many ~~such~~ reports leading to ~~the~~ final product--a "Subway Environmental Design Handbook".

The purpose of this particular report is to present, describe, and interpret the miriad of test data generated in the VST Facility for vent shafts. Junction coefficients for a wide range of vent shafts are presented and compared to theory. Recommendations are made.

17. Key Words and Document Analysis. 17a. Descriptors

*urban Transportation
environmental engineering
vents
model tests

17b. Identifiers/Open-Ended Terms

Institute for Rapid Transit (IRT)
Vent and Station Test (VST) Facility

17c. COSATI Field/Group 13F, 15E, 13A, 14B, 5E

18. Availability Statement: Releasable to the public. Available from NTIS, Springfield, Va. 22151	19. Security Class (This Report) UNCLASSIFIED	21. No. of Pages 121
	20. Security Class (This Page) UNCLASSIFIED	22. Price

VST VENT SHAFT TESTING

~~7020-6~~

AUGUST 1971

TABLE OF CONTENTS

LIST OF SYMBOLS

A	Tunnel crossectional area
A_{vi}	Inlet area of vent shaft
A_{ve}	Exit area of vent shaft
AR	Vent aspect ratio $\frac{\text{axial length}}{\text{width}}$
$C_{\Delta p}$	Upstream pressure coefficient (see p. 10)
$C_{\Delta Hs}$	Straight through loss coefficient (see p. 10)
$C_{\Delta Hc}$	Coupling loss coefficient (see p. 10)
$C_{\Delta Hi}$	Inlet loss coefficient (see p. 10)
$C_{\Delta ps}$	Vent total loss coefficient (see p. 10)
$C_{\Delta px}$	Pressure junction coefficient (see p. 10)
$C_{\dot{m}}$	Rate of mass flow coefficient (see p. 9)
c_f	Friction factor of tunnel wall
D	Tunnel diameter
ΔHi	Inlet head loss
ΔHs	Straight through head loss
ΔHc	Coupling head loss
h_e	Vent inlet axial length
L	Tunnel length
$\dot{m}_1$	Rate of mass flow upstream of vent in tunnel
$\dot{m}_2$	Rate of mass flow downstream of vent in tunnel
$\dot{m}_v$	Rate of mass flow through vent shaft
l_s	Scoop length
l_i	Variable inlet projection length

LIST OF SYMBOLS (cont'd)

p_1	Static pressure in tunnel upstream of vent
p_2	Static pressure in tunnel downstream of vent
p_∞	Static pressure in free atmosphere
p_o	Plenum stagnation pressure
V_1	Average velocity of flow in tunnel upstream of vent
V_2	Average velocity of flow in tunnel downstream of vent
V_{vi}	Average vent inlet velocity
V_{ve}	Average vent exit velocity
w_e	Vent inlet width
θ	Variable inlet slant angle from horizontal
ρ	Density of air

VENT SHAFT CODE SYSTEM

First digit : Aspect ratio AR

Second digit : Inlet area ratio (A_{vi}/A)

Third digit : Exit area ratio (A_{ve}/A)

Fourth digit : Symbolic number of vent shaft impedence

Aspect Ratio:		Inlet area ratio		Exit area ratio	
Code	Value	Code	Value	Code	Value
①	1/2	①	1/4	①	1/4
②	1	②	1/2	②	1/2
③	5	③	1	③	1
④	10	④	2	④	2
				⑥	1.5

SYMBOLS (cont'd)

Impedance:

Code	Level of Impedance
①	Lowest $C_{\Delta ps}$ (without grid $C_{\Delta ps} = 0\ (1)$)
③	Intermediate $C_{\Delta ps}$ (corse grid $C_{\Delta ps} = 0\ (10)$)
⑤	High $C_{\Delta ps}$ (fine grid $C_{\Delta ps} = 0\ (20)$)

Parameters:

$$\lambda_o = \frac{\Delta H}{\frac{1}{2}\rho V_1^2}$$

K_o = 1.05 (experimental constant)

K_i = 0.965 (experimental constant)

$$S_o = \frac{A_{v_i}}{A}\sqrt{\frac{C_{\Delta p}}{C_{\Delta p_s}}} \quad \text{(outflow)}$$

$$S_i = \frac{A_{v_i}}{A}\sqrt{\frac{C_{\Delta p}}{C_{\Delta p_s}}} \quad \text{(inflow)}$$

1. INTRODUCTION

A quantitative knowledge of the flow in "T" junctions (Figure (1)) of varying characteristics is essential in numerous areas of engineering. This problem, as it relates to the behavior of subway vent shafts, is the subject of this report.

Previous studies (references (6) and (7)) were conducted in water at lower Reynolds' numbers for the specific case of circular/circular "T" junctions. These studies failed to provide means for determining the mass flow "split-up" at the junction as a function of junction geometry, impedance, static pressure, etc., and only considered the static pressure rise (or drop) across the junction assuming the split-up to be known a-priori. The results of these studies are therefore of little direct use in subway vent shaft analysis, where vent geometries, impedance, and environment vary enormously from system to system.

Any theoretical approach to the prediction of air and heat motion within subway systems requires accurate information regarding the proportion of flow ejected through the vent shaft relative to that approaching it and the resulting pressure changes for a given set of near field conditions. In general, the flow within the neighborhood of the vent shaft is exceedingly complex and thus not readily amenable to purely theoretical analysis. As will be seen from the discussion in subsequent sections, the flow structure in the vent shaft is dominated by large scale flow separations in the case of outflow Figure (2a), and substantially influenced by persistent vortex surfaces in the case of inflow Figure (2b). Despite this complex nature, it turns out

that the global behavior of a large variety of realistic vent shaft geometries is predictable within required engineering accuracy on the basis of semi-empirical analytical considerations provided that these vent shafts do not depart radically from the "T" inlet geometry depicted in Figure (1). The analytical foundations of this prediction method are described in the following.

In the present study, the foundations of vent shaft junction theory is developed and verified on the basis of extensive experimental studies covering a large range of relevant vent shaft junction properties.

2. ANALYSIS

An analytical approach to the prediction of vent shaft behavior was put forth by DSI-AT in reference (1). While this method has turned out to be fundamentally sound, subsequent experimentation at DSI-AT has suggested certain modifications regarding the manner in which the final equations are presented, in addition to empirical corrections to the purely theoretical results. These modifications are reflected in the development given below. Since, as described in the preceeding section, the vent shaft behavior for inflow and outflow are fundamentally different, it is convenient to handle these cases separately.

2.1 Outflows

While it has already been noted that the actual flow into a vent shaft is exceedingly complex, involving large separated zones and flow non-uniformities, analytical treatment becomes possible only when a simplified model of this flow is postulated. It turns out that the errors resulting from such a simplistic model can be rectified through the incorporation of semi-empirical observations, provided that the model allows for sufficient generality.

The theoretical model selected for outflow is shown in Figure (3). As can be seen from Figure (3), one-dimensional axial flow upstream and downstream of the vent shaft is assumed, and that while flow non-uniformities can exist between stations (1) and (2), the flow quickly readjusts to a uniform profile a short distance downstream of the vent shaft. The flow remaining in the tunnel is separated from that exiting through the vent shaft by a dividing streamline. In this model, the total head of the flow is the same on both sides

of this dividing streamline. Since the velocity V_1+ is greater than V_2 for a constant area tube, the static pressure p_2 must be larger than p_1, owing to the flow diffusion effect. This is shown in the pressure plot in Figure (3).

For the flow entering the vent shaft, it is assumed that an inlet head loss ΔH_i is suffered because the fluid cannot negotiate a sharp right angled turn. It is further assumed that before entering the miter turns* the flow readjusts to a uniform profile. After being processed by the series of miter turns, the flow suffers an additional head loss ΔH_s which is identical to that which would result if ideal inlet conditions preceded the miter turns, as shown in Figure (3b). It is assumed that ΔH_s is readily computable from standard handbook data or can easily be determined from simple experiments, and is therefore a known quantity in the analysis. Thus ΔH_s becomes the first order impedance property of the vent shaft, called the "straight-through" head loss.

Now, while this simple concept of rapid flow readjustment to a uniform profile is analytically helpful, it is well known that initial flow non-uniformities do persist over great distances and take a long time to readjust. Thus, in actual fact, the velocity profile at A_{v_i} will be far from uniform, and hence the ΔH_s value actually obtained will be significantly different from that computer (or measured) on the basis of ideal or "straight-through" inlet conditions, since the manner in which the miter turns "process" the flow will depend on the actual

+Velocities V_1 and V_2 are taken as average values across the tunnel. $\frac{1}{2}\rho V^2$ is the average tunnel dynamic head.

*While the miter turns are exemplified in the figure, virtually any loss-producing components (e.g. screens, grids, sudden expansions, straight pipe wall friction, etc., or combinations thereof) could be substituted without loss of generality.

characteristics of the inlet velocity profile at A_{v_i}. This coupling between inlet and "straight-through" loss will result in an increment (or decrement, but this is not likely to be the case, since a non-uniform flow dissipates more energy) in the straight-through loss, which will be denoted by ΔH_c.

Finally, the total head dissipated at the exit of the vent shaft by free-jet action is simply $\frac{1}{2}\rho V_{ve}^2$.

Summarizing, the total energy dissipated within the flow entering the vent shaft is

$$\left[\Delta H_i + \Delta H_s + \Delta H_c + \frac{1}{2}\rho V_{ve}^2\right]$$

The energy equation for the flow entering the vent shaft (i.e. the region above the dividing streamline) is, for incompressible one-dimensional flow:

$$p_1 + \frac{1}{2}\rho V_1^2 - \left[\Delta H_i + \Delta H_s + \Delta H_c + \frac{1}{2}\rho V_{ve}^2\right] = p_\infty \qquad (1)$$

Now,

$$\Delta H_c\,,\ \Delta H_s = f\,(V_{v_i}^2)$$

But, experiments have indicated definitely that the inlet loss coefficient is dependent mainly on the axial velocity in the tunnel preceding the vent shaft, i.e.,

$$\Delta H_i = f\,(V_1^2)$$

This functional dependence is taken into account in the following normalizations defining the various loss coefficients

$$C_{\Delta H_s} = \frac{\Delta H_s}{\frac{1}{2}\rho V_{v_i}^2}$$

$$C_{\Delta H_c} = \frac{\Delta H_c}{\frac{1}{2}\rho V_{v_i}^2}$$

$$C_{\Delta H_i} = \frac{\Delta H_i}{\frac{1}{2}\rho V_1^2}$$

Also defining the driving static pressure coefficient $C_{\Delta p}$ as:

$$C_{\Delta p} = \frac{p_1 - p_\infty}{\frac{1}{2}\rho V_1^2}$$

equation (1) becomes

$$C_{\Delta p} + 1 = \left[C_{\Delta H_s} + \left(\frac{V_{ve}}{V_{v_i}}\right)^2 + C_{\Delta H_c}\right]\left(\frac{V_{vi}}{V_1}\right)^2 + C_{\Delta H_i} \qquad (2)$$

Defining

$$C_{\Delta H_s} + \left(\frac{V_{ve}}{V_{v_i}}\right)^2 = C_{\Delta p_s} = \frac{p_o - p_\infty}{\frac{1}{2}\rho V_{v_i}^2}$$

where p_o is the total pressure in the stagnation chamber preceding the ideal inlet in Figure (3b), equation (2) becomes

$$C_{\Delta p} + 1 = (C_{\Delta p_s} + C_{\Delta H_c})\left(\frac{V_{vi}}{V_1}\right)^2 + C_{\Delta H_i} \qquad (3)$$

Defining the mass flow coefficient $C_{\dot{m}}$ as

$$C_{\dot{m}} = \frac{\dot{m}_v}{\dot{m}_1} = \frac{A_{v_i}}{A}\frac{V_{v_i}}{V_1}$$

equation (3) may be solved to obtain $C_{\dot{m}}$ as follows:

$$C_{\dot{m}} = \frac{A_{v_i}}{A}\sqrt{\frac{1 + C_{\Delta p} - C_{\Delta H_i}}{C_{\Delta p_s} + C_{\Delta H_c}}} \qquad (4)$$

This is the fundamental equation used to interpret and unify the experimental data.

Consider now the flow beneath the dividing streamline (i.e., the flow that remains in the tunnel). Assume, for the purpose of this simple analysis that little total head loss is suffered along the streamlines between stations (1) and (2). It is evident that this is not actually the case, however, the flow in this region is likely to be sufficiently complex to defy simple analysis. Thus, neglecting these losses for the moment, and using the loss-free Bernoulli equation to ideally characterize the problem,

$$p_1 + \frac{1}{2}\rho V_1^2 = p_2 + \frac{1}{2}\rho V_2^2$$

so that

$$\frac{p_2 - p_1}{\frac{1}{2}\rho V_1^2} = C_{\Delta p_x} = C_{\dot{m}}(2 - C_{\dot{m}})$$

where $C_{\Delta p_x}$ characterizes the rise in static pressure between stations (1) and (2).

Let us now inquire into the magnitude of this pressure rise in relationship to an equivalent number of unvented tunnel diameters. The pressure loss coefficient in L/D of unvented tunnel is

$$(C_{\Delta p_x}) = 4\,c_f\left(\frac{L}{D}\right)$$

so that the equivalent tunnel length corresponding to the flow diffusion is

$$\left(\frac{L}{D}\right)_{equiv.} = \frac{1}{4\,c_f}\,C_{\dot{m}}(2 - C_{\dot{m}})$$

For typical value of $c_f = 0.01$, the table below gives the equivalent tunnel lengths as a function of $C_{\dot{m}}$

$C_{\dot{m}}$	0	.2	.4	.6	.8	1.0
$(L/D)_{equiv.}$	0	9	16	21	24	25

Thus, for the smaller mass flows, an error in predicting $C_{\Delta p_x}$ is not likely to lead to significant errors in overall system flow prediction. However, in the case of closely spaced vent shafts (e.g. the CTA) the accumulated error can be significant.

2.2 Inflow

With inflow, the dividing stream surface (Figure 4) is also a surface of concentrated vorticity as a result of the fact that the total heads of the flows on either side of it are, in general, different. Experience has demonstrated that such surfaces of concentrated vorticity tend to diffuse very slowly into the rest of the flow, and hence cause the flow to be disturbed from equilibrium far downstream of the vent shaft. Therefore the "near field" of an inflowing vent shaft extends for long distances downstream of the shaft itself.

In dealing with inflowing vent shafts, it is useful to define three stream-wise stations as shown in Figure (4). Station (1) is immediately upstream of the shaft, station (a) is hypothetical point where the flow begins to mix, and station (2) is the theoretical downstream boundary of the near field where the flow is uniform.

Just for the moment, let us assume that we can neglect the losses in the mixing region between (a) and (2). Applying Bernoulli's equation to the tunnel flow, between (1) and (2), we obtain

$$p_1 + \frac{1}{2}\rho V_1^2 = p_2 + \frac{1}{2}\rho V_2^2$$

Defining

$$C_{\dot{m}} = \frac{\dot{m}_v}{V_2 A}$$

$$C_{\Delta p_x} = \frac{p_1 - p_2}{\frac{1}{2}\rho V_2^2}$$

$$C_{\Delta p_x} = C_{\dot{m}}\,(2 - C_{\dot{m}}) \qquad (5)$$

Now, let us repeat this analysis using the momentum theorem, which will reflect the influence of the mixing losses. Since the inflow from the vent shaft enters the tunnel with zero tunnel-directed momentum, we may write simply

$$p_1 + \rho V_1^2 = p_2 + \rho V_2^2$$

from which we obtain

$$C_{\Delta p_x} = 2\,C_{\dot{m}}\,(2 - C_{\dot{m}}) \qquad (6)$$

which is exactly twice the pressure drop given by equation (5) which neglected the losses.* Thus, a full 50% of the pressure drop results from mixing far away from the vent shaft, and downstream at station (a), the pressure is roughly half-way between p_1 and p_2. The average pressure acting on the inlet face of the vent shaft must therefore be fairly close to p_1.

The flow induced through the vent shaft is given by the energy equation

$$p_\infty - C_{\Delta H_S}\,\frac{1}{2}\rho V_{v_i}^2 = p_1 + \frac{1}{2}\rho V_{v_i}^2$$

$$\frac{p_\infty - p_1}{\frac{1}{2}\rho V_2^2} = (1 + C_{\Delta H_S})\left(\frac{V_{v_i}}{V_2}\right)^2$$

$$C_{\dot{m}} = \frac{A_{v_i}}{A}\sqrt{\frac{C_{\Delta p}}{C_{\Delta p_S}}} \qquad (7)$$

2.3 Summary of Parameters

The definitions of relevant parameters are summarized below:

Outflow	Inflow
$C_{\dot{m}} = \dfrac{\dot{m}_v}{A V_1}$	$C_{\dot{m}} = \dfrac{\dot{m}_v}{A V_2}$

*It is noted that the equivalent tunnel diameter errors discussed in section 2.1 will also double.

$$C_{\Delta p} = \frac{p_1 - p_\infty}{\frac{1}{2}\rho V_1^{\,2}} \qquad C_{\Delta p} = \frac{p_\infty - p_1}{\frac{1}{2}\rho V_2^{\,2}}$$

$$C_{\Delta p_s} = \frac{p_o - p_\infty}{\frac{1}{2}\rho V_{v_i}^{\,2}} \qquad C_{\Delta p_s} = \frac{p_\infty - p_o}{\frac{1}{2}\rho V_{v_i}^{\,2}}$$

$$C_{\Delta p_x} = \frac{p_2 - p_1}{\frac{1}{2}\rho V_1^{\,2}} \qquad C_{\Delta p_x} = \frac{p_1 - p_2}{\frac{1}{2}\rho V_2^{\,2}}$$

Where, for both outflow and inflow, V_{v_i} is the vent shaft velocity corresponding to the vent shaft cross-sectional area A_{v_i} at the intersection of the vent shaft and tunnel (Figures (3) and (4)).

It is noted that all outflow coefficients are normalized on the basis of upstream conditions, while all inflow coefficients are related to downstream conditions. If this form were not used, and we alternatively normalized both inflow and outflow coefficients on (for example) upstream conditions, then the mass flow and driving pressure coefficients would blow up for the case of $V_1 = 0$, which corresponds to $\dot{m}_v = \dot{m}_2$ (all of the flow enters through the vent shaft). Thus, in order to avoid these difficulties, the above format is used throughout.

3. THE VST FACILITY

The VST (Vent and Station Test) facility was designed to evaluate the performance of vent shafts with inflow and outflow. The details of the design are contained in Appendix A, and will not be reproduced here. The facility is designed to permit the determination of the straight through pressure loss $C_{\Delta p_s}$ of an arbitrary vent shaft geometry for inflow and outflow as shown schematically in Figure (5) as well as the "in-situ" behavior of the vent shaft as sketched in Figure (6). The procedures for straight-through and in-situ testing are described individually below. Supplementary information can be found in reference (2).

3.1 Straight-Through Tests - Outflow (Figure (5a))

In this case the vent shaft is located on a secondary plenum mounted on the main plenum of the VST facility. Flow supplied from the blowers enters a carefully formed inlet duct located in the main plenum and is filtered by a 100 mesh screen before encountering a 12 tube integrating pitot-static rake. Survey of velocity distribution across the inlet duct at the rake location showed the flow to be uniform to within ± 5%. of the average maximum velocity. The integrating rake averages these errors and yields a total entering mass flow measurement estimated to be within ± 2% accuracy. After leaving the inlet duct, the flow enters the secondary plenum and is filtered through another 100 mesh screen to insure that stagnation conditions will be closely approximated in the upper volume of the plenum. Large fairings are provided at the inlet to each and every vent shaft to produce the required ideal inlet for the vent shafts. Typical examples of inlet flow uniformity as obtained from velocity surveys in the inlets are shown in Figure (7). The total pressure driving the flow across the vent shaft is measured in the upper volume of the secondary plenum by means of an alcohol micromanometer. Each vent shaft was tested at three inlet velocities, and the resulting $C_{\Delta p_s}$ values of the three runs were averaged (typically they varied less than 10% from one another). The straight-through loss is computed as follows:

$$C_{\Delta p_s} = \frac{p_o - p_\infty}{\frac{1}{2}\rho {V_{v_i}}^2}$$

3.2 Straight-Through Tests - Inflow (Figure (5b))

As with outflow, the vent shaft is mounted on the secondary plenum. The flow entering from the atmosphere in the inlet to the vent shaft due to the simulated ground surface* and subsequently travels through the vent shaft and is exhausted into the upper portion of the secondary plenum. It is then filtered through a 100 mesh screen and allowed to settle in the lower portion of the secondary plenum before entering a 5.5 to one area ratio contraction nozzle. The combination of the screen, flow settling and acceleration in the nozzle has the effect of producing uniform flow in the exit of the nozzle, where a pitot static tube is located. Velocity surveys confirmed that the flow was uniform

*Since most subway vent shafts emerge flush with the ground, each vent shaft tested was fitted with a large flat surface to simulate this situation.

to within ± 5% over a wide range of vent shaft sizes. The $C_{\Delta p_s}$ value was obtained at three velocities according to the equation.

$$C_{\Delta p_s} = \frac{p_\infty - p_o}{\frac{1}{2}\rho {V_{v_i}}^2}$$

The results at the three velocities were averaged.

3.3 In-Situ Tests - Outflow (Figure (6a))

Flow supplied by the blowers was filtered through a series of 100 mesh screens in the plenum chamber and entered the pipe through a screened fairing to insure a uniform velocity profile at the inlet of the pipe. The turbulent pipe flow profile was allowed to develop naturally in the 22 diameters of pipe upstream of the vent shaft. A fully developed turbulent pipe flow mean velocity profile existed just upstream of the vent shaft as shown in Figure (8). The disturbance in the profile produced by the outflow causes the flow downstream of the vent shaft to be non-uniform. Another 28 diameters is provided to allow the profile to re-establish. This mass flow upstream of the shaft is measured 5 diameters downstream of the pipe inlet by an integrating pitot rake connected to a micromanometer. The downstream mass flow is measured 26 diameters downstream of the vent shaft by another integrating pitot rake connected to a micromanometer. The difference between these two mass flows is that which flows out of the vent shaft. The mass flow coefficient is computed as follows:

$$C_{\dot{m}} = \frac{\dot{m}_v}{\dot{m}_1} = \frac{\dot{m}_1 - \dot{m}_2}{\dot{m}_1} = 1 - \frac{\dot{m}_2}{\dot{m}_1} = 1 - \sqrt{\frac{\Delta p_2}{\Delta p_1}}$$

where Δp is the difference between the integrated total pressure and the local static pressure. This procedure was verified by numerically integrating velocity surveys across the upstream and downstream locations for a number of different cases and comparing these results with the integrating rake results.*

The local static pressure at the vent shaft location is a function of the tunnel losses downstream of the vent shaft. These were simulated by means of an "ETL" (effective tunnel loss) valve located at the discharge end of the VST facility. By varying this value, the driving pressure coefficient

$$C_{\Delta p} = \frac{p_1 - p_\infty}{\frac{1}{2}\rho V_1^2}$$

and hence $C_{\dot{m}}$ could be varied throughout a large range $0 \leq C_{\dot{m}} \leq 1$.

To know exactly where to measure p_1 required a knowledge of the axial pressure distribution along the tunnel in the near field of the shaft. For this reason, pressure taps were located every 1/4 diameter along the pipe in this neighborhood and the pressure distributions were displayed on inclineable water multimanometers. A typical plot of static pressure variation is shown in Figure (9). Regions A and B correspond to pressure gradients produced by wall friction in the usual way, except that since the profile downstream of vent shaft is disturbed for a few diameters, the slope of the pressure drop per dynamic head is greater than exists upstream. Eventually this drop asympotes to the value in A. In the near field of the vent

* The average dynamic head is taken as $\frac{1}{A}\int_0^{2\pi}\int_0^{R} \frac{1}{2}\rho V^2 r \, dr \, d\theta$
(See page 35)

shaft (between (1) and (2)), the static pressure rises from 1 to 2 owing to the diffusion of the flow remaining in the pipe as described in the preceding section. The driving pressure coefficient consistent with this analysis was the one selected in the experiments, i.e.,

$$C_{\Delta p} = \frac{p_1 - p_\infty}{\frac{1}{2}\rho V_1^2}$$

As illustrated in the figure, the pressure rise coefficient was taken as

$$C_{\Delta p_x} = \frac{p_2 - p_1}{\frac{1}{2}\rho V_1^2}$$

3.4 In Situ Tests - Inflow (Figure (6b))

The in-situ inflow tests were conducted in a similar manner to the outflow ones, except for a couple of specific items. For inflow, a formed inlet was placed at the inlet to the pipe so that the flow entering from the atmosphere would do so uniformly. The ETL valve could no longer be used to control the upstream tunnel losses, and hence the pressure level at the vent location since it introduced severe non-uniformities in the flow. Therefore changeable loss-producing grids were submitted to produce the required results. The mean velocity profile immediately upstream of the vent shaft location closely approximates the fully developed turbulent pipe flow profile as shown in Figure (10).

The axial static pressure distribution (Figure (11) in the neighborhood of the inflowing vent shaft was found to be less predictable than in the case of outflow, apparently owing to an inflow separation as shown in Figure (2). In any case, the downstream extent of the near field for inflow was considerably greater than for outflow, as has already been anticipated on the basis of arguments presented in section 2.

In the case of inflow, all vent shaft parameters are normalized on downstream conditions for the reasons given in section 2. Thus,

$$C_{\Delta p} = \frac{p_\infty - p_2}{\frac{1}{2}\rho V_2^{\,2}}$$

$$C_{\Delta p_x} = \frac{p_1 - p_2}{\frac{1}{2}\rho V_2^{\,2}}$$

$$C_{\dot m} = \frac{\dot m_v}{\dot m_2} = \frac{\dot m_2 - \dot m_1}{\dot m_2} = 1 - \frac{\dot m_1}{\dot m_2} = 1 - \sqrt{\frac{\Delta p_1}{\Delta p_2}}$$

Where Δp_1 and Δp_2 are given from the upstream and downstream integrating pitot static rakes as before. The use of the integrating rakes was also verified for inflow as described in section 3.3.3.

4. EXPERIMENTAL APPROACH

In view of the fact that subway vent and blast shaft geometries vary enormously from system to system, it became immediately obvious that little would be served by constructing and experimentally evaluating a long number of specific shaft geometries. Rather, it was deemed sensible to try to fundamentally understand, on the basis of the theory of the preceding section supplemented by a series of special control vent shaft tests, the foundations of vent

shaft behavior with a view towards obtaining universal analytical tools capable of predicting the performance of arbitrary vent shaft geometries.

While the geometries of vent shafts vary endlessly, the analysis of the preceding section indicates that relatively few parameters actually characterize the system, at least to a first order approximation. Expressing this dependence functionally, (for the general inflow/outflow conditions)

$$C_{\dot m} = f\left(C_{\Delta p_s},\ {}^{A_{v_i}}/A,\ C_{\Delta p},\ C_{\Delta H_c} \text{ or } C_{\Delta H_i}\right)$$

Now, ${}^{A_{v_i}}/_A$ is a known geometrical property. $C_{\Delta p}$, the driving pressure coefficient is known (usually implicitly) in any subway environmental calculation procedure insofar as the vent shaft is concerned. In principle $C_{\Delta p_s}$, the straight-through loss coefficient can be calculated on the basis of standard handbook data for turns, contractions, expansions, inlets, etc. In practice this generally is not so straightforward as will be seen from the discussion later on in section 5.5. The inlet/straight-through loss coupling coefficient $C_{\Delta H_c}$ which appears only in the outflow equation must be determined from experiments performed with the actual vent shaft in place in the tunnel since it is dependent upon vent shaft geometrical details and their effect on the entering flow from the tunnel into the vent shaft.

The theory described in the previous section is actually a very simplistic description of an enormously complex flow situation, and therefore cannot be expected to yield reliable predictions without the benefit of empirical modification.

4.1 Straight Control Vent Shafts

In order to verify the general applicability of the theory, and to supply the empirical corrections as required, an experimental control vent shaft program was devised. These vent shafts varied widely in geometry (A_{v_i}/A and $\mathcal{R}$) as shown in Figure (12). The $C_{\Delta p_s}$ values for each of these vent shafts could be changed simply by changing the grids. The grids simulated (to a first approximation) the total effect of vent shaft internal losses from turns, sudden contractions and expansions, wall friction, etc. The equivalent of 30 vent shafts differing in $C_{\Delta p_s}$, $\mathcal{R}$, and A_{v_i}/A could be synthesized in this way. The data obtained in this manner was used to verify and empirically adjust the theoretical results.

4.2 Plenum Vent Shafts

However, there still remained the question of whether or not the grids did, in fact, faithfully represent internal losses which result from typical subway vent shaft geometries, and consequently, whether or not a correlation based on "gridded" vent shafts would equally well predict realistic vent shaft geometries. This was investigated by radically changing the method of achieving $C_{\Delta p_s}$. These vent shafts were selected and the exit plenums shown in Figure (13) were installed on each of the three. The $C_{\Delta p_s}$ values were varied as a function of the sudden expansion losses in the plenum and by varying the exit area of the plenum to that of the inlet area of the vent shaft. These plenum vent shafts were tested with and without grids. It was found that these data were in reason-

able agreement with the simple "gridded" vent shafts for the higher $C_{\Delta p_s}$ values (see further discussion in section 5.1 and 5.2).

4.3 Miter Turn Vent Shafts

However, since both the "gridded" and plenum vent shafts exhausted in a direction perpendicular to the tunnel flow, it was decided to construct a family of miter-turn vent shafts which discharged parallel to the tunnel flow, either in the upstream and downstream direction, and sideways (Figure (14)). This was done throughout a range of vent exit to inlet area ratios, thereby producing a corresponding range of $C_{\Delta p_s}$. Since many subway vent shafts have series of miter turns, this family of vent shafts constitutes another step in the direction of generalizing the results to arbitrary geometries.

4.4 Effect of Tunnel Cross-Section

Thus far in our experimental considerations, we have been concerned only with the effects of vent shaft geometry on the behavior of the shafts. Test were also performed to determine the influence of tunnel cross sectional geometry on vent shaft performance.

The three cross sectional geometries illustrated in Figure (15) were tested. In all cases, the vent shaft geometries were kept the same, i.e.,

$$\mathcal{R} = \frac{A_{v_i}}{A} = \frac{A_{v_e}}{A_{v_i}} = 1$$

4.5 Variable Inlet

It has been suggested that various approaches can be adopted to improve the aerodynamic efficiency of vent shafts. One such approach has already been used in the design of the WMATA subway system vent shafts, as shown schematically in Figure (16). The idea here is to diffuse the tunnel flow so as to increase the effective driving pressure coefficient at the vent shaft location, as well as decrease the inlet loss. The pertinent question is, what angle is optimum? One might also inquire into the influence of flow scoops as shown in Figure (16), and as to whether vent inlets optimized for outflow behave acceptably under inflow conditions. (In some cases, vent shafts are required to operate efficiently in both modes whereas, for example, in the case of blast shafts, they are not.)

To answer these questions, a variable inlet $\frac{A_{v_i}}{A} = 1$ vent shaft mounted on a square tunnel cross section was tested as shown in Figure (16), with and without flow scoops for outflow and inflow, for a range of grid-produced straight-through loss coefficients of $6.5 \leq C_{\Delta p_s} \leq 17$, and $\theta = 8^\circ$, 18°, 45°, and 90°. In addition, the circular fairing inlet depicted in the figure was tested for comparison. The results of these tests are described in section 6. The limiting cases of $\theta = 0$ and $0 = 90^\circ$ are also shown in the figure.

4.6 Miter Turn Internal Loss Coefficients

Many subway vent shaft geometries consist of a series of miter turns. In general, the inlet area of the miter is different from its exit area, i.e., $A_e/A_i \gtrless 1$ as shown in Figure (17).

In order to compute the $C_{\Delta p_s}$ value of such a vent shaft, it is necessary

to have experimental data on the loss coefficients of miter turns of arbitrary A_e/A_i. An extensive literature search (reference (3)) failed to find data for geometries other than $A_e/A_i = 1$.

In reference (4) it was assumed (for lack of better data) that a variable area miter turn would be simulated as depicted in Figure (17a). One might inquire as to why the method of Figure (17b) might not give equivalent results, and of course it doesn't because of the different dynamic head distributions.

Since, in general, the variable area miter turn is an important component of subway vent shafts, it was decided to perform limited experiments to determine the variation of loss coefficient $C_{\Delta H}$ with A_e/A_i over the range of area ratio values $1/8 \leq A_e/A_i \leq 2$ the variable area miter turn test rig is shown in Figure (18). The results are presented in section 5.5. It is noted that these results are of limited applicability since the aspect ratio h/w of the exit changed throughout a range $1/8 \leq h/w \leq 2$, while the inlet cross-section was always square. According to reference (5), the loss coefficient is relatively insensitive to aspect ratio, in the range $h/w < 1$, but is increasingly affected by $h/w \geq 1$.

The total head loss was determined in the following (conventional) manner.

$$C_{\Delta H} = \frac{\Delta H}{\frac{1}{2}\rho V_2^{\,2}} = \frac{p_o - p_\infty}{\frac{1}{2}\rho V_2^{\,2}} - 1 - \left(f_D \frac{L_D}{h_D} + f_i \frac{L_i}{h_i} \right)$$

where f is the friction factor of the rectangular mixing duct as obtained from reference (8). In all cases, the duct length was maintained at a minimum value of $\frac{L_D}{h_D} = 10$ to insure complete pressure recovery after the turn. This was especially important for the case of $A_e/A_i > 1$. Velocity profiles were taken along the duct to verify that this condition was attained at the duct exit. This data is presented in section 5.5.

5. RESULTS & DISCUSSION

5.1 Mass Outflow: $C_{\dot{m}} = f(C_{\Delta p})$

Equation (4) theoretically describes the behavior of a vent shaft with outflow. The value of $C_{\Delta H_i}$ appearing in the numerator under the radical is unknown. $C_{\Delta H_i}$ physically represents the percentage of exiting tunnel flow kinetic energy which is lost in negotiating the turn into the vent shaft. If all of this kinetic energy is lost, then $C_{\Delta H_i} = 1$. The experiments performed in the VST facility show that $C_{\Delta H_i}$ does in fact assume a value closely approximating unity for all "T"-junction vent shafts tested regardless of internal vent shaft geometry. Therefore, equation (4) reduces to the following expression

$$C_{\dot{m}} = K_o \frac{A_{v_i}}{A} \sqrt{\frac{C_{\Delta p}}{C_{\Delta p_s} + C_{\Delta H_c}}} \qquad (8)$$

where the constant K_o has been inserted as an empirical correction factor close to unity.

Now, the remaining unknown quantity $C_{\Delta H_c}$ physically represents

the coupling between inlet and straight-through losses, and would be expected to be sensitive to vent shaft internal loss and physical geometry.

For the case of the straight control vent shafts where internal losses were produced exclusively by grids, $C_{\Delta H_c}$ was experimentally correlated as a function of the vent shaft inlet geometry as follows:

$$C_{\Delta H_c} = C \left(\frac{A_{v_i}}{A}\right)^{0.35} (Æ)^{0.15} \quad , \quad C = 0.45 \qquad (9)$$

where $Æ = \frac{\text{length of vent shaft along tunnel}}{\text{width of vent shaft}}$

For the plenum and miter vent shafts, C was found to be significantly less than 0.45 indicating that the geometric details as to how the internal losses are produced determine $C_{\Delta H_c}$. This, of course, was to be expected based on the discussions above.

Theoretically, the fact that the "constant" C varied with the type of vent shaft in an unknown manner would be gounds for concern. Fortunately, in practice this produces little problem. The reason for this is that $C_{\Delta H_c}$ appears in the linear combination $(C_{\Delta H_c} + C_{\Delta p_s})$ in equation (4) and since in practical vent shaft configurations, $C_{\Delta p_s} >> C_{\Delta H_c}$, the latter can be neglected for engineering intents and purposes. As an example, take the case where

$$\frac{A_{v_i}}{A} = Æ = 1$$

and the highest value of C observed in the tests was,

$$C = 0.45$$

so that $$C_{\Delta H_c} = 0.45$$

according to the correlation given above. If the vent shaft had no internal losses whatsoever, the corresponding value of $C_{\Delta p_s}$ would be unity. Since $C_{\Delta H_c}$ is nearly half this value, the influence of $C_{\Delta H_c}$ as given by equation (8) would represent a reduction in $C_{\dot{m}}$ of about 20%. However, actual vent shafts possess significantly higher values of $C_{\Delta p_s}$ than the ideal vent shaft described above. According to reference (4), the lowest $C_{\Delta p_s}$ value for an existing subway vent shaft is on the order of $C_{\Delta p_s} = 5.0$, (with the average being on the order of 10), so that, all else remaining constant, neglecting $C_{\Delta H_c}$ entirely would influence the value of $C_{\dot{m}}$ computed from equation (8) by only 4.5% in this case. In most existing vent shafts the $C_{\Delta p_s}$ values are usually somewhat higher, so that the presence of $C_{\Delta H_c}$ can in practical applications be ignored. However, with very large ${}^{A_{v_i}}/_{A}$ vent shafts with small impedance, this approximation may not be satisfactory.

The data plotted in the next section is in terms of

$$S_o = \frac{A_{v_i}}{A} \sqrt{\frac{C_{\Delta p}}{C_{\Delta p_s}}} \quad \text{vs.} \quad C_{\dot{m}}$$

so that the $C_{\Delta H_c}$ effect in equation (8) is ignored. As established previously, this will in general result in poor correlations for the case of $C_{\Delta p_s} = 1.0$ (no internal losses), but the correlation will improve for the more realistic higher values. Thus at very low vent shaft impedance, there exists a non-trivial geometry influence which tends to vanish as the vent shaft internal losses increase.

5.1.1 Straight Vent Shafts

Figures (19a), (20), and (21) show $C_{\dot{m}}$ vs. S_o plots for the straight vent shafts for grid-produced $C_{\Delta p_s}$ values of 1.0, 6.5, and 17.0 respectively. As anticipated previously, the $C_{\Delta p_s} = 1.0$ plots (no grids) are poorly correlated, whereas the $C_{\Delta p_s} = 6.5$, and 17.0 are very well correlated and described by equation (8) with $C_{\Delta H_c} = 0$. Figure (19b) shows the $C_{\Delta p_s} = 1.0$ data correlated by the inclusion of $C_{\Delta H_c}$ as given by equation (9), where K_o assumes a value of 1.05 for all straight vent shafts tested.

5.1.2 Plenum Vent Shafts

Figures (22), (23), and (24) show the plenum vent shafts for the various values of $C_{\Delta p_s}$, achieved through the use of grids and/or variations in ${}^{A_{v_e}}/_{A_{v_i}}$ and different plenum geometries as described in Appendix B.

It is seen that these results correlate reasonably well with the straight vent shafts, but the slope K_o assumes a somewhat lower value ($K_o \approx 1.0$) than it had with the straight vent shafts. However, the slope seems to be independent of the value of $C_{\Delta p_s}$ or the manner in which $C_{\Delta p_s}$ is achieved. Also, a slight non-linearity in the curve is noted in these tests.

5.1.3 Miter Turn Vent Shafts

Three miter-turn vent shafts were investigated which differed in exit-to-inlet area ratio ${}^{A_{v_i}}/_{A_{v_e}}$. These area ratios were ${}^{A_{v_i}}/_{A_{v_e}} = 0.5$, 1.0, and 2.0. Each of these vent shafts were tested exhausting in the upstream and downstream directions relative to the tunnel flow (Figure (14)). The A_{vi}/A_{ve} = 1.0 miter was tested exhausting to the side at 90° to the tunnel flow for comparison. In all cases, the inlet area/tunnel area ratio was held constant at $\frac{A_{v_i}}{A}$ = 1 with $\mathcal{R}$ = 1.0.

In all cases at least 10 channel heights of miter exit duct length were provided so that the exiting flow could reestablish after the sharp miter turn before exhausting to the atmosphere. This aspect of the miter is discussed in more detail in section 5.5. The miter turn vent shaft data is plotted in Figure (25) where the corresponding values of $C_{\Delta p_s}$ are given. It is seen that the slopes of the $C_{\dot{m}}$ - S_o curves retain the same value (K_o = 1.05) as that observed for the straight vent shafts, but that the downstream discharge curve is displaced downward as in the case of the plenum vent shafts. The upstream and side-discharge miter exhibits no such pronounced shift.

Since the miter data is reasonably well correlated by equation (8) with $C_{\Delta H_c}$ = 0, one is encouraged to expect that arbitrary replica vent shaft geometries would be similarly tractable. The fact that the upstream and downstream discharging miters exhibit these characteristic shifts should not constitute a basis for serious concern because:

a) The shifts are relatively small (-10% in $C_{\dot{m}}$)

b) Virtually all real subway vent shafts discharge in a direction normal to the tunnel flow.

5.2 Mass - Inflow; $C_{\dot{m}} = f(C_{\Delta p})$

The mass-inflow equation was derived in section (2) as

$$C_{\dot{m}} = K_i \frac{A_{v_i}}{A} \sqrt{\frac{C_{\Delta p}}{C_{\Delta p_s}}} \tag{10}$$

where K_i has been inserted as an empirical correction factor close to unity.

Letting

$$S_i = \frac{A_{v_i}}{A} \sqrt{\frac{C_{\Delta p}}{C_{\Delta p_s}}}$$

$$C_{\dot{m}} = K_i \, S_i \tag{11}$$

5.2.1 Straight Vent Shafts

Figures (26), (27), and (28) show plots of $C_{\dot{m}}$ vs S_i for nominal $C_{\Delta p_s}$ values of 1.0, 6.5, and 17.0. It is noted the curves are linear and pass through the origin as predicted by equation (11). The value of K_i determined from these data is

$$K_i = 0.965$$

It is noted that in the case of inflow, no correlation scatter is found for the low $C_{\Delta p_s}$ as was the case for outflow (Figure (19a)). The reason is, that the flow in the vent shaft (which determines $C_{\Delta p_s}$) in the case of inflow is unaffected by the tunnel flow and depends only upon the local static pressure acting across the face of the shaft at the vent/tunnel junction. Thus the flow enters the vent shaft at its intake uniformly (unlike the outflow condition), and no coupling coefficient $C_{\Delta H_c}$ exists, which is responsible for the correlation scatter at small $C_{\Delta p_s}$ as seen in Figures (19a) and (19b).

5.2.2 Plenum Vent Shafts

Figures (29), (30), and (31) demonstrate that equation (11) correctly describes the behavior of all plenum geometries tested and that the slope $K_i = 1.06$ remains unchanged. This confirms the fact that the manner of achieving $C_{\Delta p_s}$ does not effect the validity of equation (11).

5.2.3 Miter-Turn Vent Shafts

Figure (32) shows the ability of equation (11) to correlate the miter turn vent shaft data. It is seen that in the case of inflow, the difference between upstream, downstream, and sideways discharge does not influence the correlation substantially, as it did in the case of outflow.

5.3 Static Pressure Change $C_{\Delta p_x}$

5.3.1 Outflow

The simple theory of section 2 assumed that diffusion of the tunnel flow from ①→② took place without losses in total head. Obviously, there must be some loss because the tunnel flow is significantly disturbed by the outflow.

Taking these losses into account, the following relationships apply to outflow

$$C_{\Delta p_x} = C_{\dot{m}} (2 - C_{\dot{m}}) - \lambda_o$$

where $\lambda_o > 0$ is a total head loss coefficient defined by

$$\lambda_o = \frac{\Delta H}{\frac{1}{2} \rho V_1^2}$$

λ_o is an unknown quantity which is probably a function of $C_{\dot{m}}$ as well as vent shaft geometrical details. Qualitatively, the effect of this loss is to reduce the magnitude of the pressure differential $p_2 - p_1$. Thus we would expect that for outflow, the experimental points would fall <u>below</u> the theoretical values. This is seen to be the case in Figures (33) through (35). It is noted that considerable scatter in the data is evident. Extensive repeat runs have verified that this is <u>not</u> experimental error, but rather, must be attributed to a requirement for further parameterization to unify the experimental points.

The best fit curve of these data yield the following semi-empirical relationships.

$$C_{\Delta p_x} = 1.067\, C_{\dot{m}} (1.5 - C_{\dot{m}})$$

The theoretical curves

$$C_{\Delta p_x} = C_{\dot{m}} (2 - C_{\dot{m}})$$

are plotted for comparison.

The $C_{\Delta p_x}$ variation with $C_{\dot{m}}$ for the plenum and miter vent shafts showed precisely the same behavior as the straight vent shafts, so that little purpose is served in presenting this data.

In view of the highly complex nature of the flow in this region, and the fundamental simplicity of the theory, the $C_{\Delta p_x}$ correlations presented must be considered to be acceptable.

5.3.2 Inflow

In section 2 it was found that for the case of inflow, the pressure drop coefficient was given by

$$C_{\Delta p_x} = 2\,C_{\dot{m}}\,(2 - C_{\dot{m}})$$

(i.e., exactly twice the value of the outflow pressure rise due to the presence of the vortex surface mixing).

This equation is compared with the experimental data in Figures (36), (37), and (38). It is seen that the agreement is reasonable.

Also included for comparison is the best experimental data fit equation for all $C_{\Delta p_s}$ values

$$C_{\Delta p_x} = 1.92\,C_{\dot{m}}^{0.4}$$

5.4 Effects of Tunnel Cross-Section on Vent Shaft Behavior

Three different tunnel cross section geometries were tested, all with

$$\frac{A_{v_i}}{A} = \text{Æ} = 1.0$$

and throughout a range of grid-produced loss coefficients

$$1.0 < C_{\Delta p_s} < 23$$

These cross sections and associated vent geometries are shown in Figure (15).

A direct comparison of results for outflow and inflow are given in Figures (39) and (40) respectively. It is seen that while the pure circular cross section tends to yield somewhat better performance than the other two (especially the square section at small S_o), one cannot distinguish a systematic difference in the case of inflow. For outflow, the difference is significant enough to justify a correction. This can be roughly accomplished by taking

$$K_o = 1.0 \text{ for the circular X-section with roadbed}$$

and

$$K_o = 0.88 \rightarrow 0.92 \text{ for the square cross section}$$

K_i retains its value of

$$K_i = 0.965$$

which has already been determined in section 5.2.

The roadbed cross section and vent shaft configuration is the one which is being incorporated in DSI-IRT's SAT (Subway Aerodynamic Test Facility).

5.5 Variable Area Miter Turn Loss Coefficients - Computation of $C_{\Delta p_s}$ -

The results obtained for the head loss in a changing area miter turn as determined according to the methods of section 5.2.3 are shown in Figure (41). It is seen that the method of simulating the behavior of a miter turn by assuming that the flow turns at constant area before the contraction (or expansion) yields fairly decent correlation with the experimental results. The alternative method yields no correlation whatsoever.

Figure (42) shows the total head distributions measured in the miter mixing duct at various stations along the duct. It is seen that the miter turn produces great disturbances in the flow, and 8-10 duct heights are required before the flow re-equilibrates.

In practical subway vent shafts, where miter turns are placed in series e.g. Figure (43), the spacing between the miters cannot permit re-adaption of the flow before it enters the next miter turn. The experimental curve of Figure (41) is valid only when the inflow velocity profile upstream of the miter is uniform.

5.6 Variable Inlet

Outflow

The different geometries of variable inlet tested are shown in Figure (16). The results of the tests are shown in Figures (44), (45), and (46). The results are easily interpreted with the aid of equation (4), re-written below:

$$C_{\dot{m}} = \frac{A_{v_i}}{A} \sqrt{\frac{C_{\Delta p} + 1 - C_{\Delta H_i}}{C_{\Delta p_s}}}$$

The effect of the sloped or faired inlet is to reduce the value of the inlet loss $C_{\Delta H_i}$ to something less than unity, which is the value that was universally found

for all "T" junctions. It is noted from the above equation that;

i) When $C_{\Delta H_i} < 1$, $C_m = 0$ can be achieved with $C_{\Delta p} < 0$ (i.e., sub-atmospheric pressure upstream of the vent shaft), but that the minimum possible value of $C_{\Delta p}$ is -1.0 (for unpowered vent shafts).

ii) Since $C_{\Delta p} \rightarrow C_{\Delta p_s}$ for $C_{\Delta p_s} \gg 1$, then $C_{\Delta p} \gg (1-C_{\Delta H_i})$ for $C_{\Delta p_s} \gg 1$. Therefore, the higher the value of either $C_{\Delta p}$ or $C_{\Delta p_s}$, the less sensitive will be the vent shaft to inlet conditions. Hence, for high impedence vent shafts, little advantage can be expected to accrue from well designed inlets. On the other hand, for low $C_{\Delta p_s}$ shafts, considerable benefit can be obtained. Roughly 4% improvement can be expected with the WMATA sloped inlet design (which has a $C_{\Delta p_s}$ value of about 10 (reference (4)) over what would have been achieved with a conventional "T" junction.

These predictions are borne out by the experimental data. Figures (44) through (46) reveal that at higher values of $C_{\Delta p_s}$, very little benefit accrues from the tailored inlets. At $C_{\Delta p_s} = 1$, however, dramatic improvements in performance are achieved vis a vis the 90° junction.

While the circular fairing inlet was in general the best, the performance of the vent shafts even at small $C_{\Delta p_s}$ seems to be remarkably independent of the inlet slope angles tested (8^o , 18^o , and 45^o).

Figure (47) shows the effects of inlet scoops on the vent shaft behavior at $C_{\Delta p_s} = 1.0$. It is seen that the scoop tested seriously degrades the performance of the vent shaft over that achieved for the same shaft without the scoop.

<u>Inflow</u>

Figure (48) shows the influence of vent inlet geometry for inflow into these same vent shafts (designed for outflow). It is noted that the inlet scoop ruins the inflow into the shaft as would be expected. However, without the scoop, the sloped inlets behave only slightly more poorly then the standard "T" vent shaft at $C_{\Delta p_s} = 1.35$.

However, at a $C_{\Delta p_s} = 16.2$ value, it is seen from Figure (49) that the influence of the inlet shape is essentially lost.

6. COMMENT ON DATA REDUCTION

The experimental driving pressure coefficient results were normalized on the basis of the average transverse dynamic pressure across in the tunnel as obtained by the integrating pitot static rake.

In other words, the average dynamic head used was

$$(\Delta p)_a = \frac{1}{R}\int_0^R \Delta p \; dr$$

However, the true average dynamic pressure across the tunnel is given by

$$(\Delta p)_b = \frac{2}{A}\int_0^{\pi}\int_0^R \Delta p\,(r) \;\; dr \; d\theta$$

For the Reynold's numbers existing in the experiment, it was found that the $(^1/_9)$th power law closely described the mean velocity profile. For these conditions,

$$\frac{\Delta p_b}{\Delta p_a} = \frac{0.68\ \Delta p_{max}}{0.82\ \Delta p_{max}} = 0.83$$

Hence, the driving pressure coefficients are increased by

$$1\sqrt{\frac{1}{0.83}} = 1.10$$

over that measured by the diagonally integrating rake.

The reduced data was corrected by this factor to account for this effect, since experiments indicated that the velocity distributions over the pipe were cylindrically symmetrical.

Often the quasi-average dynamic pressure defined as

$$\Delta p_q = \frac{1}{2} \rho U_{avg}^2$$

is used as the average dynamic head. In the present study, the true average dynamic head defined as

$$p_b = \frac{2}{A} \int_0^{\pi}\int_0^{R} \Delta p\, r\, dr\, d\theta$$

is used. Defining the ratio of these two quantities as

$$K = \frac{\Delta p_q}{\Delta p_b}$$

the following table may be used to correct from one value to the other, where U is defined by the turbulent pipe flow power law profile.

$$\frac{U}{U_m} = \left(\frac{2y}{D}\right)^{1/n}$$

(see figure (8) for coordinate system).

TABLE I
DYNAMIC PRESSURE CONVERSION

n	k
7	1.02041
8	1.01602
9	1.01291
10	1.01062

It is seen that there is very little difference between these two quantities.

7. CONCLUSIONS

A theoretical analysis of the behavior of vent shafts was performed in order to rationally analyze and interpret the experimental data obtained in the program, and to provide the analytical information required for subway environmental analysis.

The equivalent of 69 different "T" junction vent shafts have been tested with inflow and outflow throughout the entire range of mass flow coefficients. These vent shafts varied widely in vent-to-tunnel area ratio, aspect ratio, tunnel cross sectional geometry, vent impedance, and method of achieving this impedance.

Fifteen vent shafts with six special inlet configurations were also studied in this program with outflow and inflow.

The internal head losses in a variable area (A_e/A_i) miter turn were also determined.

The conclusions of this study are as follows:

1. The relationships

$$C_{\dot{m}} = K_o \frac{A_{v_i}}{A} \sqrt{\frac{C_{\Delta p} + 1 - C_{\Delta H_i}}{C_{\Delta p_s} + C_{\Delta H_c}}} \qquad \text{(outflow)}$$

$$C_{\dot{m}} = K_i \frac{A_{v_i}}{A} \sqrt{\frac{C_{\Delta p}}{C_{\Delta p_s}}} \qquad \text{(inflow)}$$

correctly describe the behavior of vent shafts which essentially intersect the tunnel at 90° at the vent-tunnel junction.

In these relationships, $C_{\Delta H_c}$ is a parameter which is dependent upon the coupling between the tunnel flow and that exiting through the vent shaft. $C_{\Delta H_i}$ represents the loss in kinetic energy suffered by the tunnel flow as it enters the shaft. $C_{\Delta H_i}$ has a theoretical limit of zero for a perfectly designed inlet.

2. For "T" - junction vent shafts

a) $C_{\Delta H_i} = 1.0$

b) $C_{\Delta H_c}$ may be neglected for $C_{\Delta p_s} \gg 1$. For example, $C_{\Delta p_s} = 5$, a 4.5% error could be expected by neglecting $C_{\Delta H_c}$ for an $^{A_{v_i}}/_{A}$ = Æ = 1.0 straight-discharge vent shaft.

c) $C_{\Delta H_c}$ becomes an important, though generally unknown parameter for $C_{\Delta p_s} \longrightarrow 1.0$ (an efficient vent shaft).

d) For straight-discharge vent shaft geometries, it has been found that

$$C_{\Delta H_c} = 0.45\,(\text{Æ})^{0.35}\left(^{A_{v_i}}/_{A}\right)^{0.15}$$

Strictly speaking, it can only be claimed that this relationship is valid for a vent height-tunnel diameter $(^H/_D)$ of 4.0 which is the value tested in this program. However, limited testing appears to indicate that it is applicable for $^H/_D \geq 1$

e) The behavior of K_o varies somewhat with vent shaft internal geometry - i.e., the manner in which $C_{\Delta p_s}$ is achieved. A good average constant value of this parameter will give +5, -15 % or better accuracy in the low $C_{\dot m}$ range $(0 \leq C_{\dot m} \leq 0.25)$ and $\pm$ 5% accuracy in the high $C_{\dot m}$ range $(0.25 \leq C_{\dot m} \leq 1.0)$ for most vent shafts.

f) K_i = .965 for all vent shafts, and is independent of the manner in which $C_{\Delta p_s}$ is produced.

g) The axial static pressure rise across an outflowing vent shaft is given by the semi-empirical relationship

$$C_{\Delta p_x} = C_{\dot m}\,(2 - C_{\dot m}) \qquad \text{(theoretical)}$$

$$C_{\Delta p_x} = 1.067\,C_{\dot m}\,(1.5 - C_{\dot m}) \qquad \text{(best fit empirical)}$$

h) The axial static pressure drop across an inflowing vent shaft results from the combined mechanisms of flow acceleration and turbulent mixing along the vortex surface. Each accounts for roughly half of the pressure drop. Theory predicts the following relationship.

$$C_{\Delta p_x} = 2\,C_{\dot m}\,(2 - C_{\dot m}) \qquad \text{(Inflow)}$$

A best-fit experimental curve is

$$C_{\Delta p_x} = 1.92\left(C_{\dot m}\right)^{0.4} \qquad \text{(Inflow)}$$

3. The tunnel cross sectional geometry has a slight influence on vent shaft performance in the case of outflow, but negligible influence on inflow. The difference in the case of outflow can be accounted for by replacing the $K_o = 1.05$ value found for circular cross sections by

$$K_o = 1.0 \text{ for circular tunnels with roadbeds}$$

and

$$K_o = 0.88 \rightarrow 0.92 \text{ for square tunnels}$$

at least for the geometries tested, which were

$$\frac{A_{v_i}}{A} = AR = 1.0$$

4. a) For sloped and faired inlets, $C_{\Delta H_i}$ assumes values less than unity, yielding significant improvements in vent shaft outflow performance in the case of low impedance shafts $C_{\Delta p_s} = 0$ [1]. The benefits achieved evaporate rapidly as $C_{\Delta p_s}$ is increased. At $C_{\Delta p_s} = 10$, the sloped and faired inlets yield something on the order of a 4% performance improvement in outflow. The inflow performance is not substantially affected, especially at the higher values of $C_{\Delta p_s}$.

b) Flow scoops seriously degrade vent shaft outflow and inflow performance, at least at the lower values of $C_{\Delta p_s}$ tested. The penalty is on the order of 35% for an 18° slope/scoop inlet.

5. Since an accurate determination of $C_{\Delta p_s}$ is required for precise prediction of $C_{\dot{m}}$ and hence $C_{\Delta p_x}$, it is important to assess the reliability

of standard engineering methods in determining $C_{\Delta p_s}$ for arbitrary vent shaft geometries. The variable area miter-turn internal loss study revealed that 8 - 10 duct heights are required for the flow velocity profile to re-equilibrate and become sensibly uniform. In practical subway vent shafts consisting of a series of miter turns, on the order of one or less duct heights exists between turns. Hence, a highly non-uniform, or often even reversed profile enters the downstream miter turn after passing through the preceding miter. Under these circumstances, prediction of $C_{\Delta p_s}$ becomes intractable.

Improved vent shaft designs for subway systems can result in reduced values of $C_{\Delta p_s}$. Certainly, every effort in this direction should be made to insure optimum ventilation within the system. Unfortunately, as described previously, under these circumstances the actual performance of the vent shaft becomes more difficult to predict. Furthermore, the effect of an operating exhaust blower located in the vent shaft causes the effective $C_{\Delta p_s}$ to be greater, or less, depending on whether or not one has inflow or outflow. In the case of outflow, an exhaust fan can cause $C_{\Delta p_s}$ to be small, zero, or negative, which means that $C_{\Delta H_c}$ now becomes important, but unfortunately unpredictable even for simple geometries.

REFERENCES

1. Vent and Station Test (VST) Facility Design, DSI-AT Interim Report #UMTA-DC-MTD-7-71-11, January 1971

2. Vent and Station Test (VST) Facility Test Procedure, DSI-AT Interim Report #UMTA-DC-MTD-7-71-15

3. Research Bibliography - Ventilation and Environmental Control in Subway Rapid Transit Systems, Interim Report #UMTA-DC-MTD-7-71-2, March 1971

4. Single-Track Subway System Components - Kaiser Engineering Report, January 1971

5. Handbook of Air Conditioning, Heating, and Ventilating, Clifford Strock, Industrial Press, 1959

6. A Model for Flow Distribution in Manifolds, R. A. Bajura, ASME Paper no. 70-PWr-3, November 2, 1970.

7. Mechanics of Manifold Flow, John S. Mc Nown and M. ASCE American Society of Civil Engineers, Transactions Paper no. 2714, August, 1953.

8. Schlichting, H., Boundary Layer Theory, Mc Graw Hill, 4th Edition, 1960.

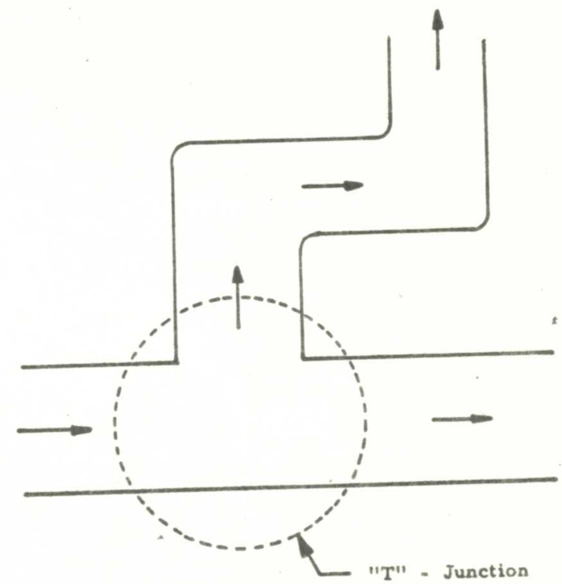

FIGURE (1)

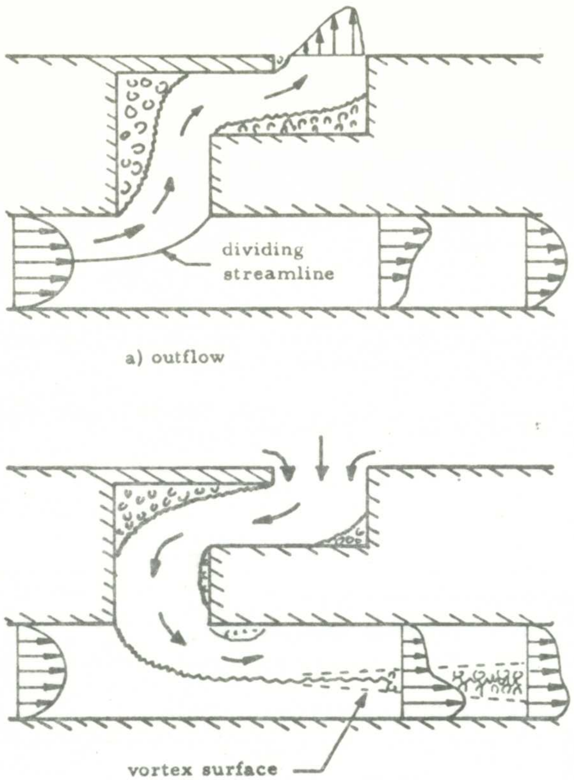

FIGURE (2)

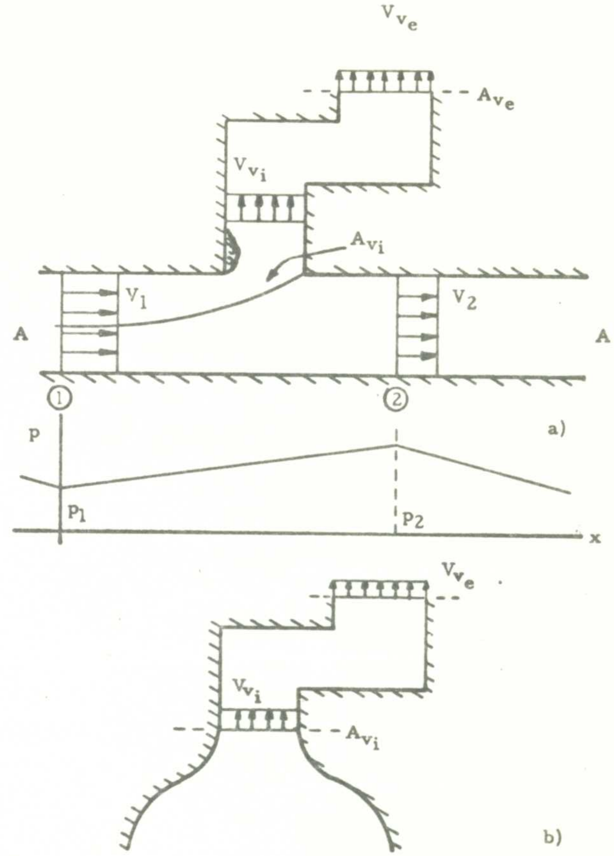

Theoretical Model for Outflow

FIGURE (3)

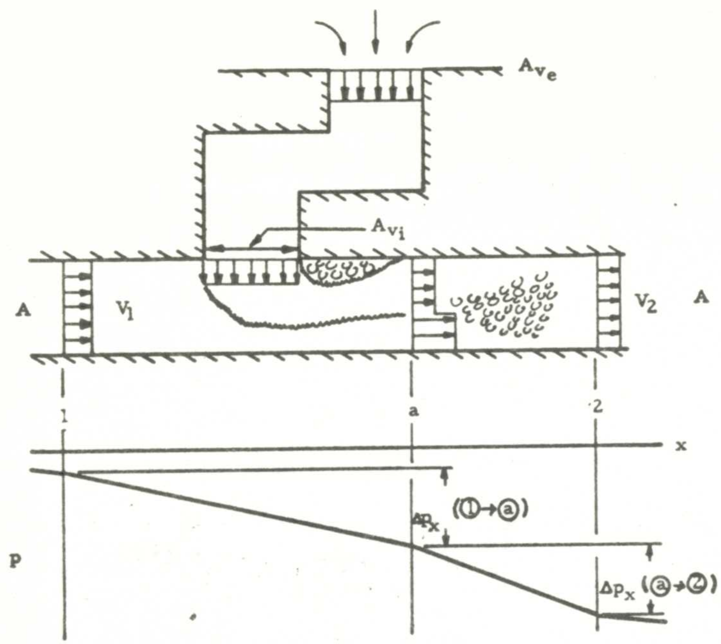

Theoretical Model of Vent Shaft with Inflow

FIGURE (4)

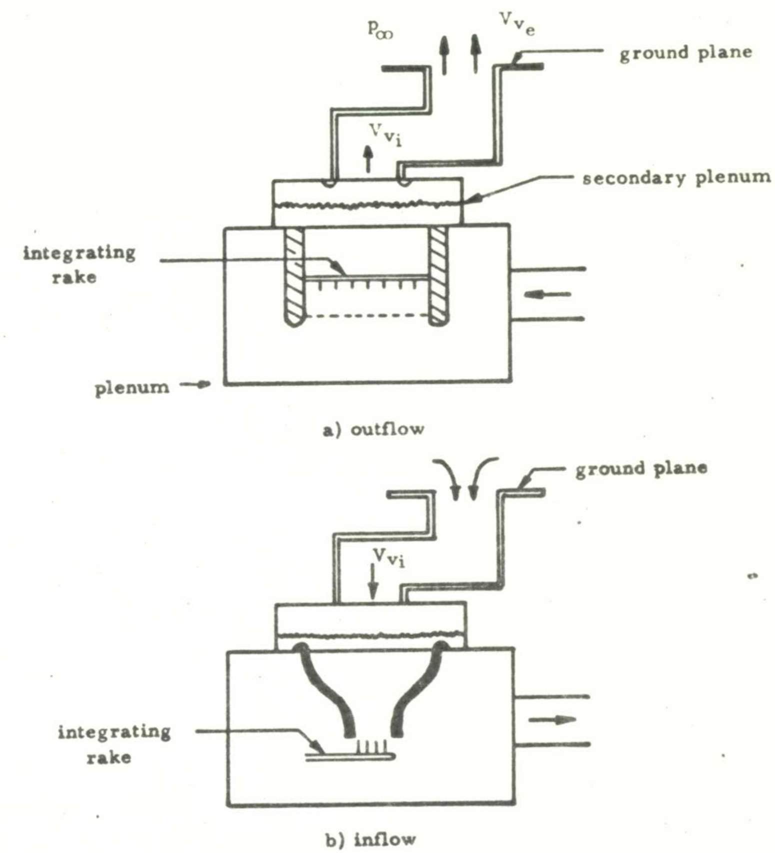

Straight Through Loss ($C_{\Delta p_s}$) Determination (Schematic)

FIGURE (5)

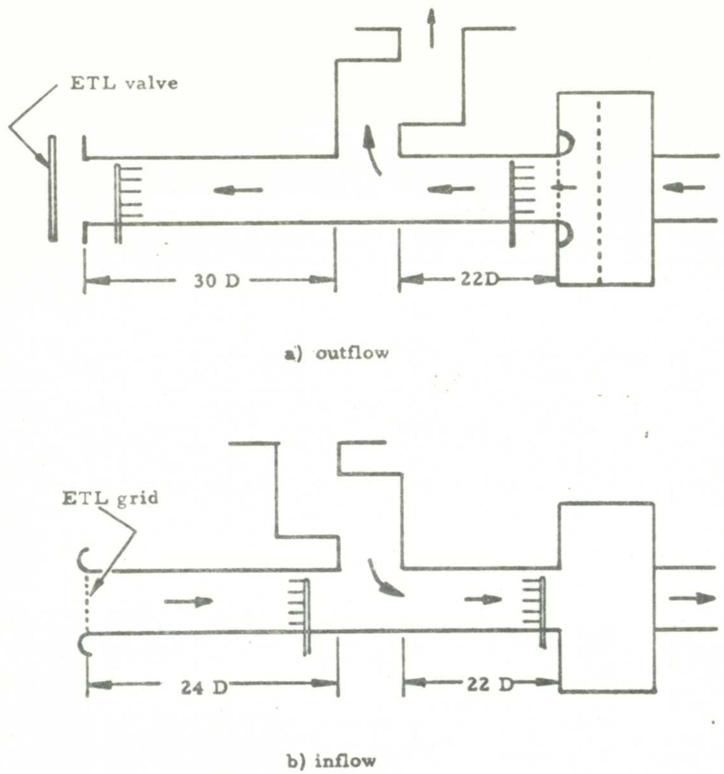

In Situ Testing (Schematic)

FIGURE (6)

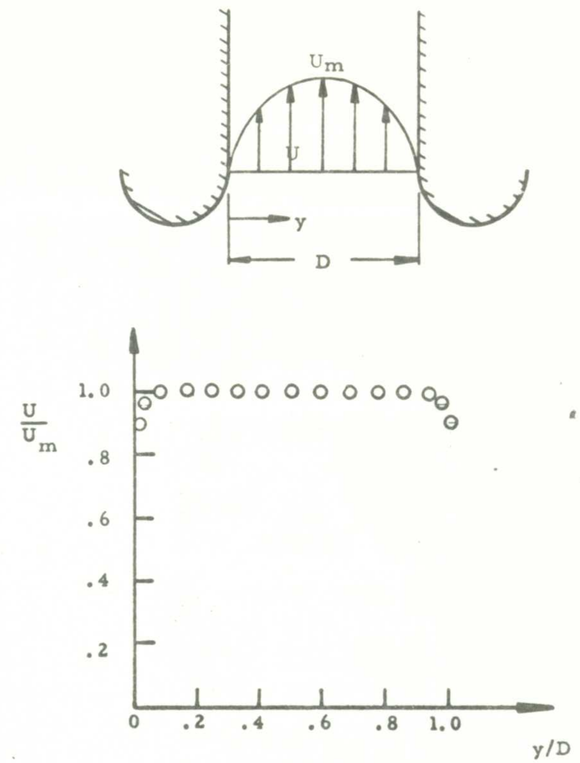

Example of Velocity Survey Across Vent Shaft #233 Inlet

In Straight Through Outflow Testing

FIGURE (7)

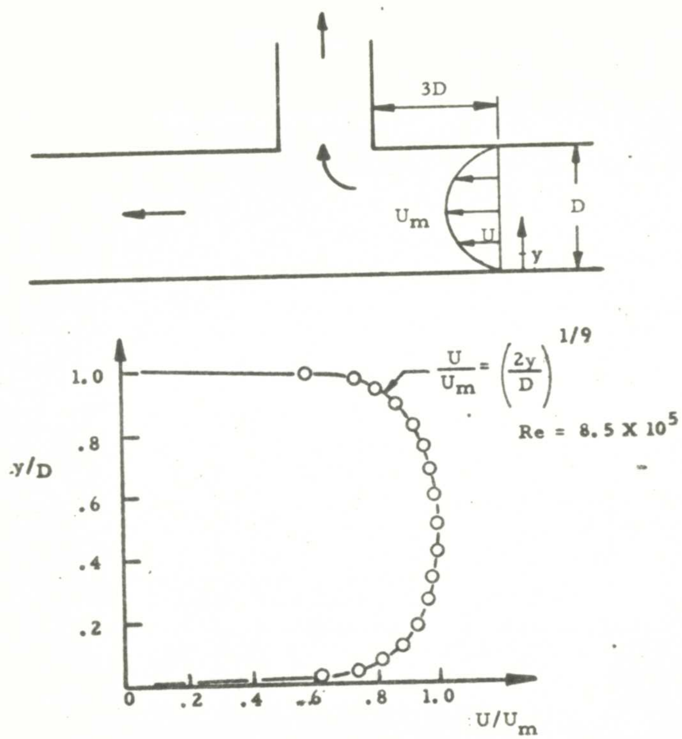

Velocity Profile Immediately Upstream of Vent Shaft (Outflow)

FIGURE (8)

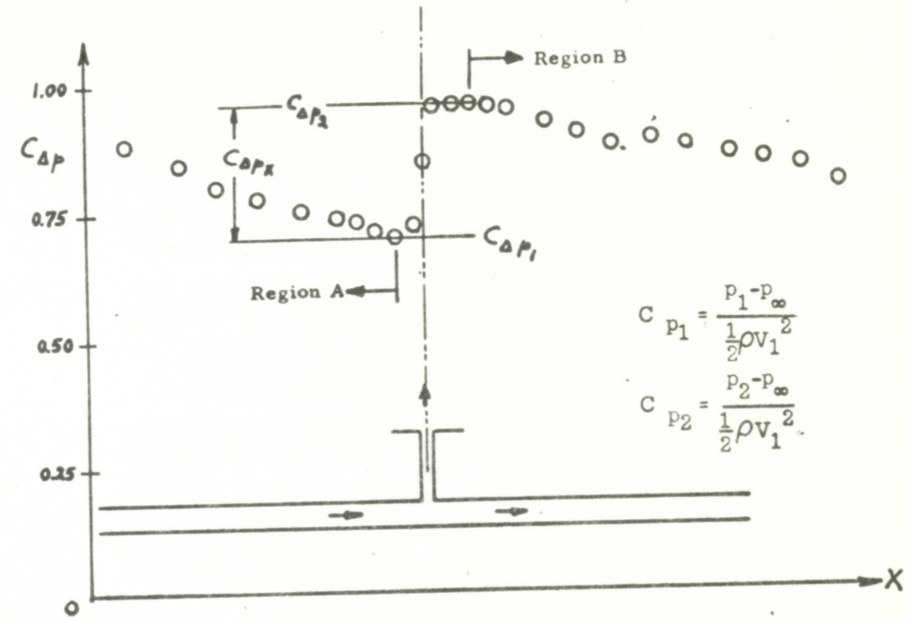

Longitudinal Pressure Distribution Across Outflowing Vent Shaft

(#1111)

$C_{\dot{m}} = 0.18$ $\quad (C_{\Delta p_x})_{expt} = 0.25$

$(C_{\Delta p_x})_{th} = 0.33$

FIGURE (9)

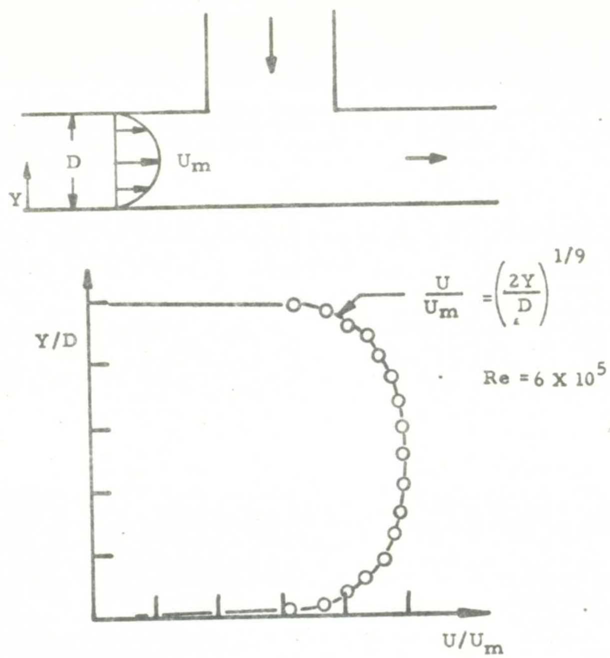

Velocity Profile Immediately Upstream of Vent Shaft (Inflow)

FIGURE (10)

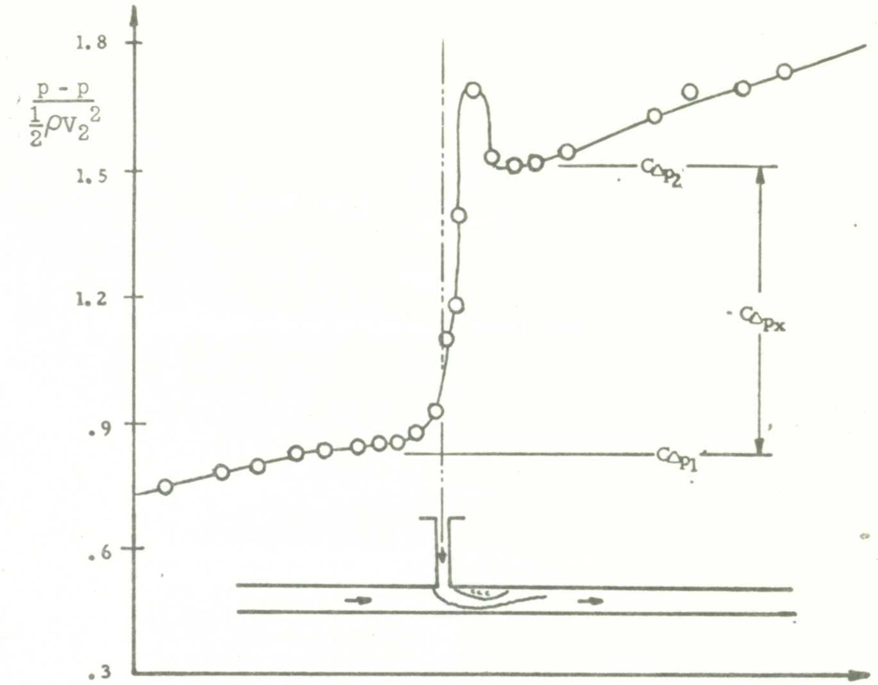

Longitudinal Pressure Distribution Across Inflowing Vent Shaft

(#1111)

$C_{\dot{m}} = 0.20$ $(C_{\Delta p_x})_{expt} = 0.70$

$(C_{\Delta p_x})_{th} = 0.72$

FIGURE (11)

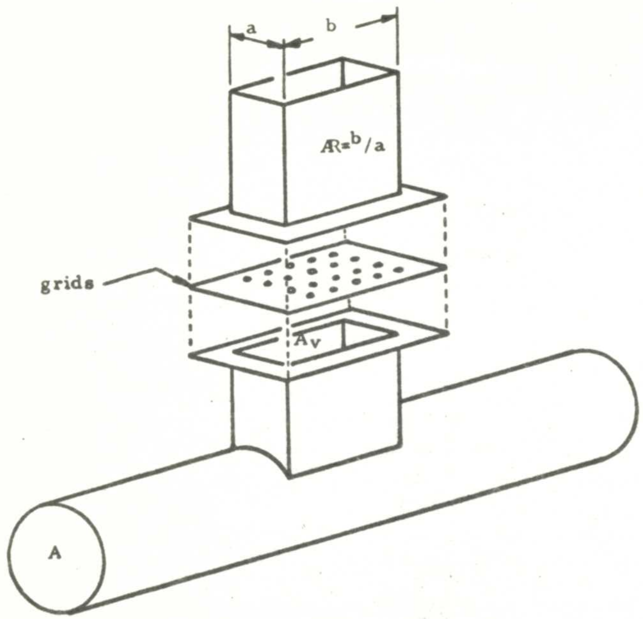

Straight Vent Shafts

FIGURE (12)

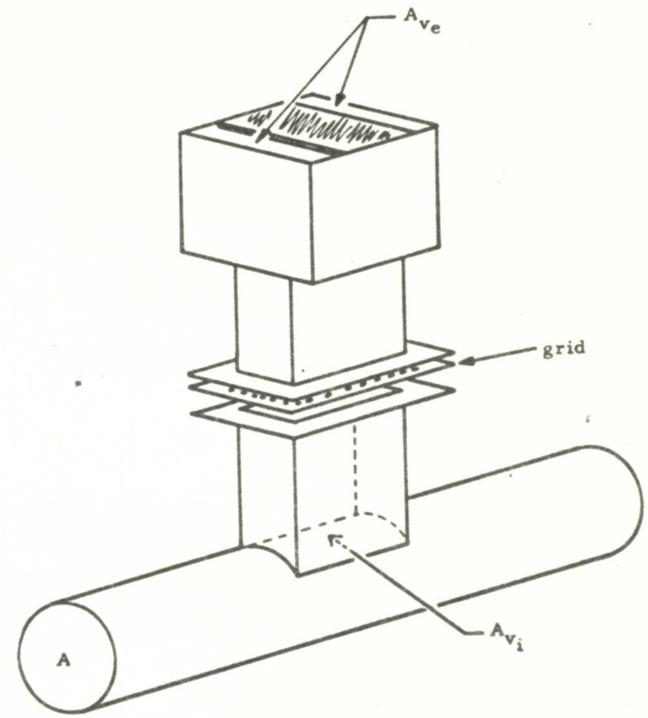

Plenum Vent Shafts

FIGURE (13)

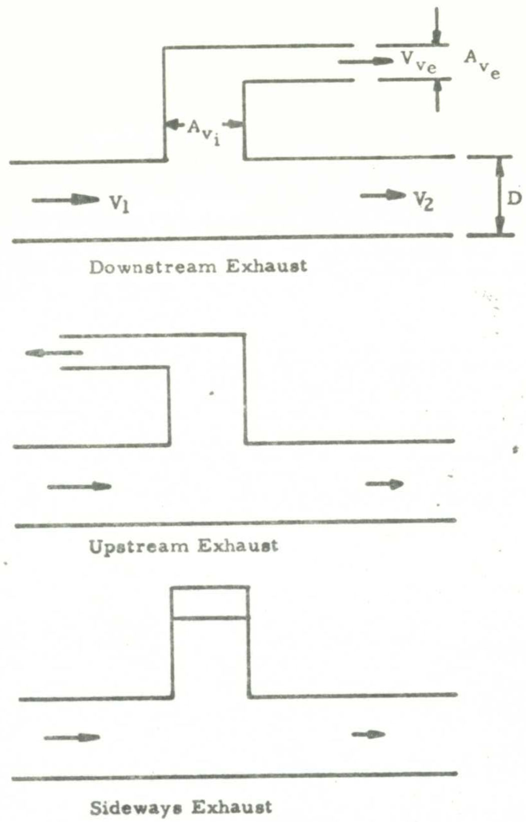

Miter Turn Vent Shafts

FIGURE (14)

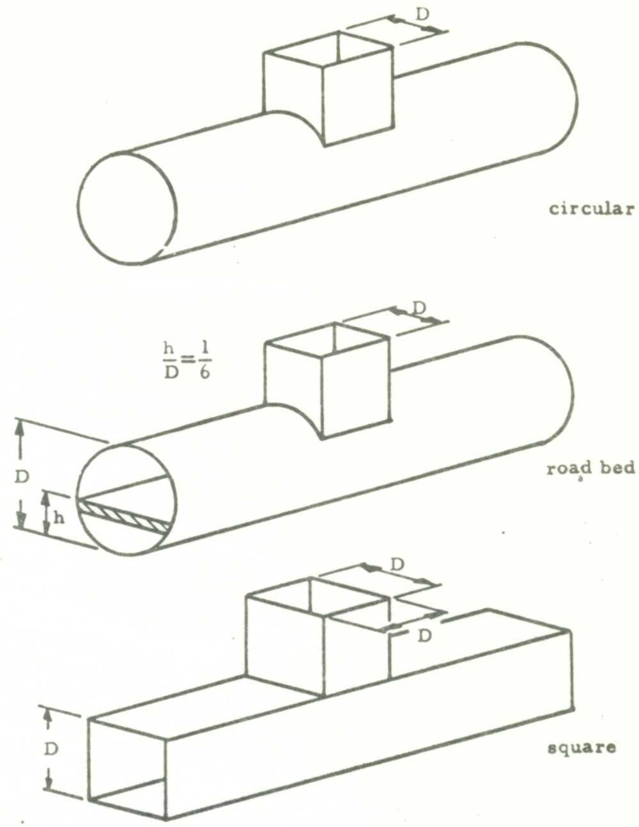

Tunnel Cross Sections Tested

FIGURE (15)

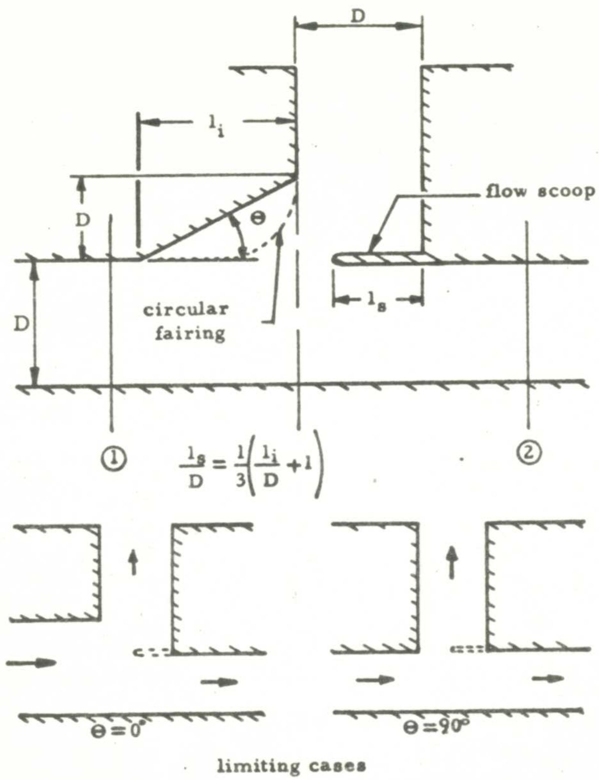

Variable Inlet

-- Experimental Configuration and Limiting Cases --

FIGURE (16)

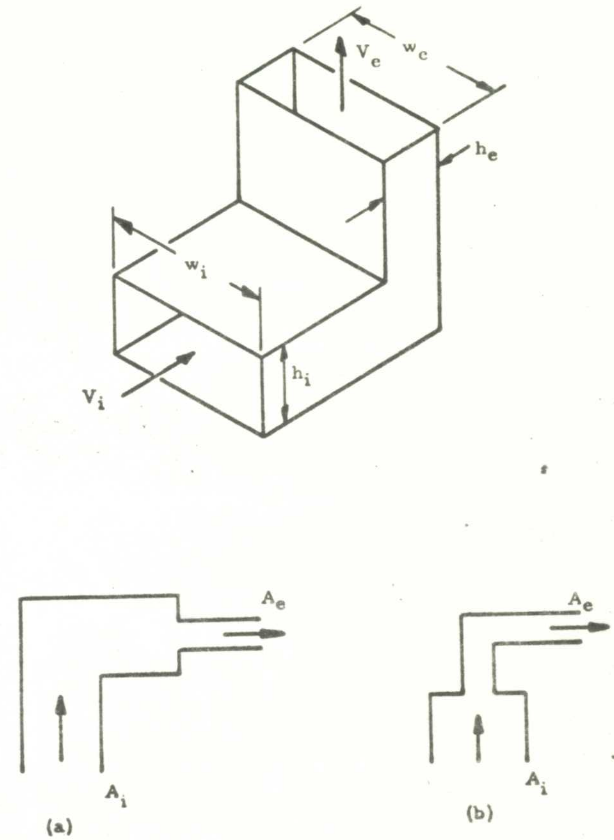

Variable Area Miter Turn

FIGURE (17)

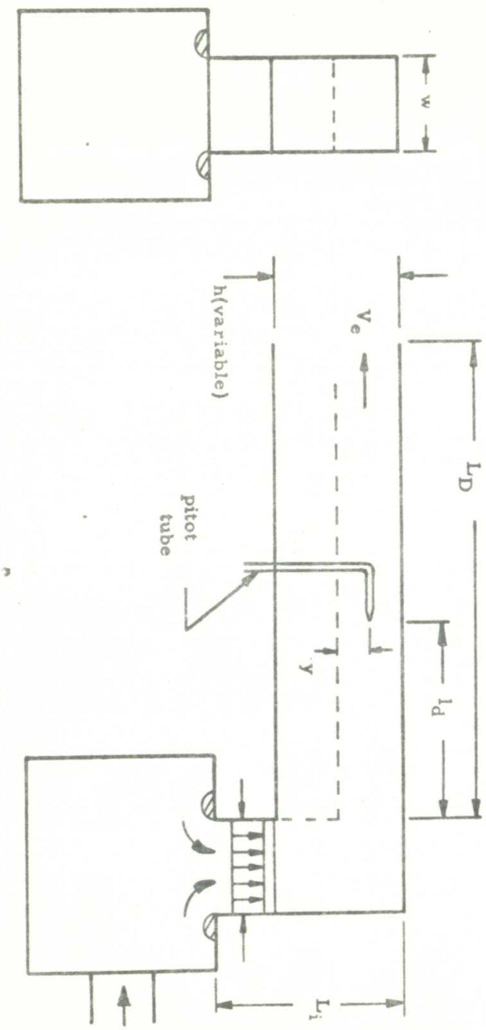

Variable Area Miter Turn Test Setup

FIGURE (18)

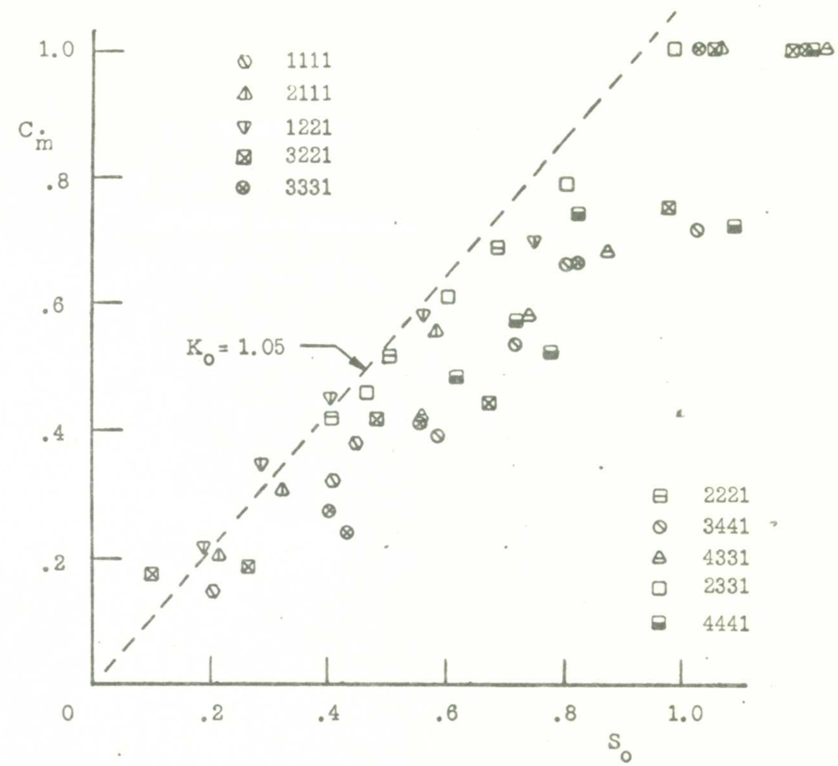

Straight Vent Shafts With Outflow

$C_{\Delta p_S} = 1.0$

$C_{\Delta H_c} = 0$

FIGURE (19a)

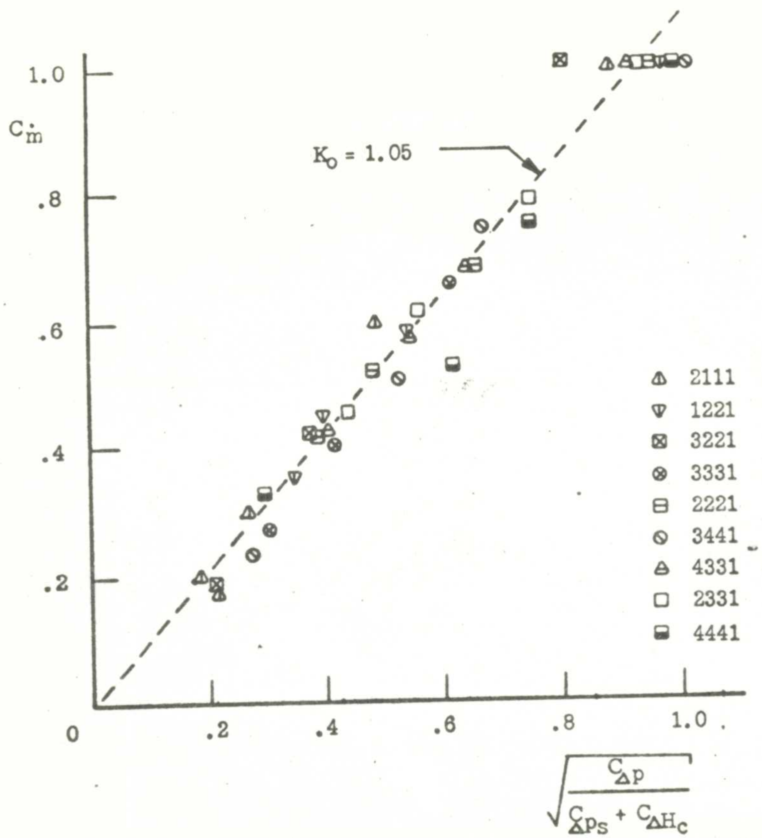

Straight Vent Shafts With Outflow

$C_{\Delta p_s} = 1.0$

$C_{\Delta H_c} = 0.45\,(AR)^{0.35}(A_{si}/A)^{0.15}$

FIGURE (19b)

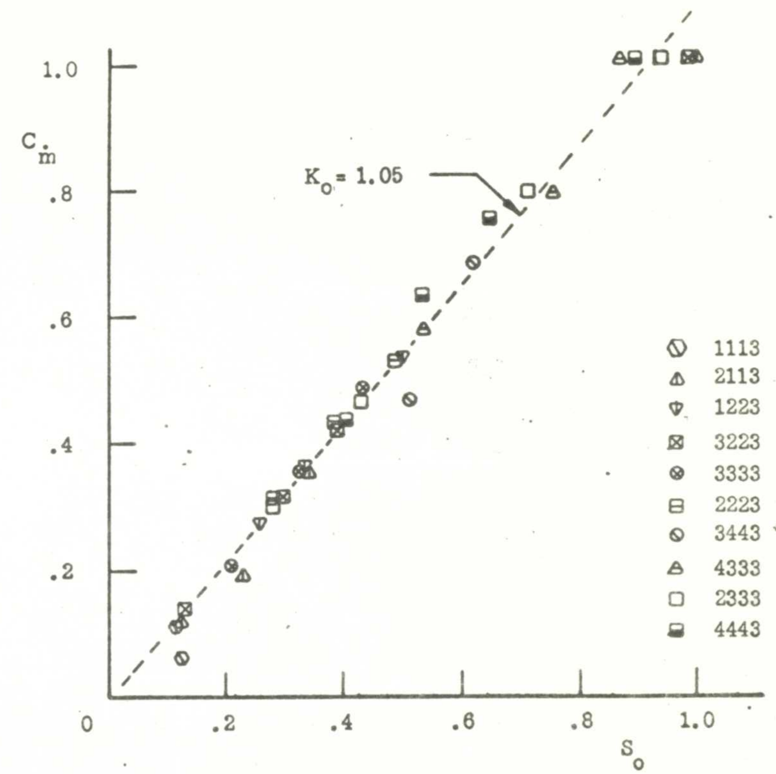

Straight Vent Shafts With Outflow

$C_{\Delta p_s} = 6.5$

FIGURE (20)

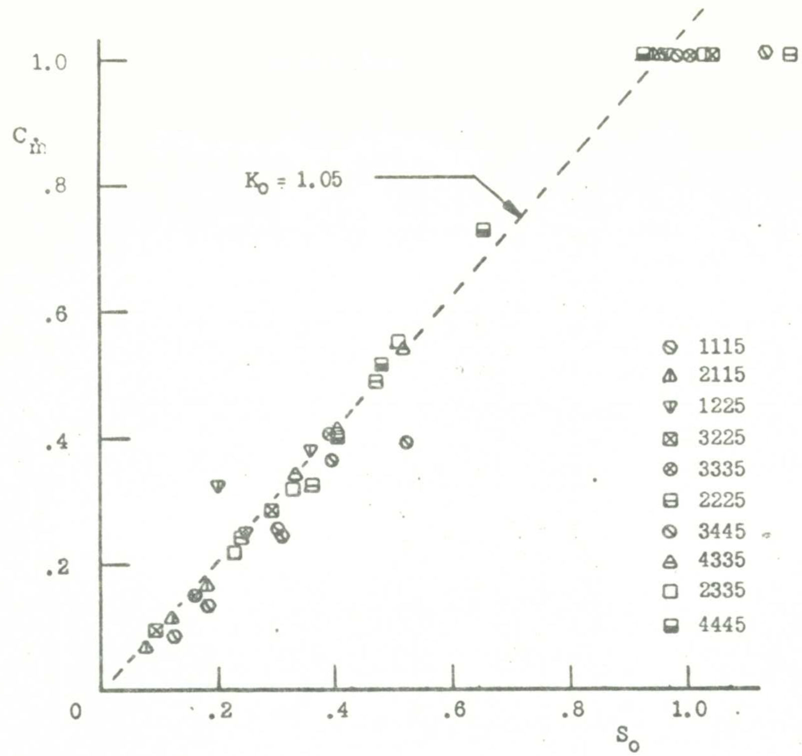

Straight Vent Shafts With Outflow

$C_{\Delta P_s} = 17.0$

FIGURE (21)

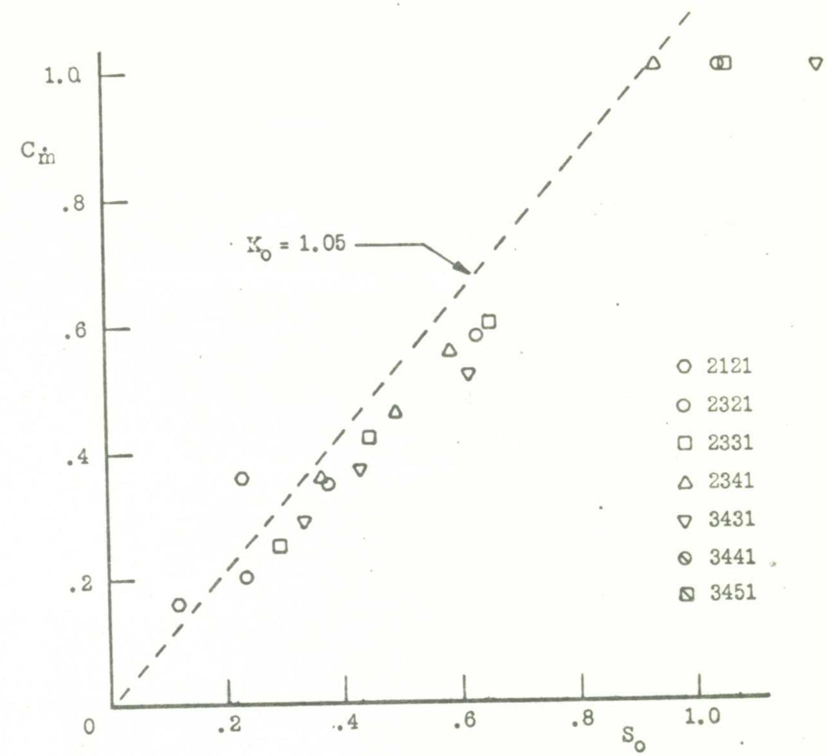

Plenum Vent Shaft With Outflow

FIGURE (22)

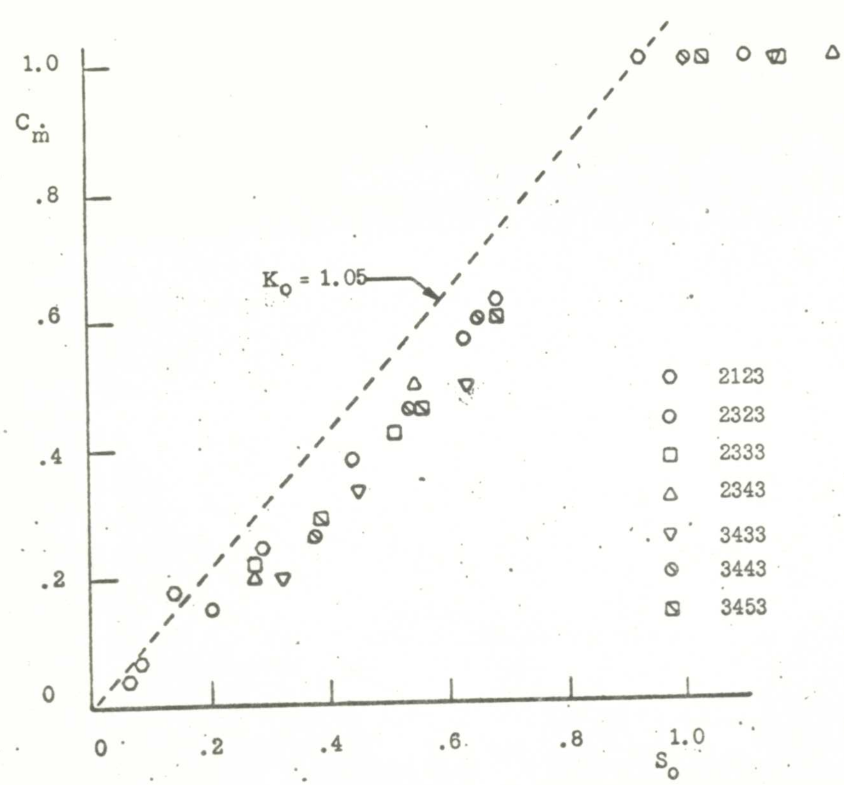

Plenum Vent Shaft With Outflow

FIGURE (23)

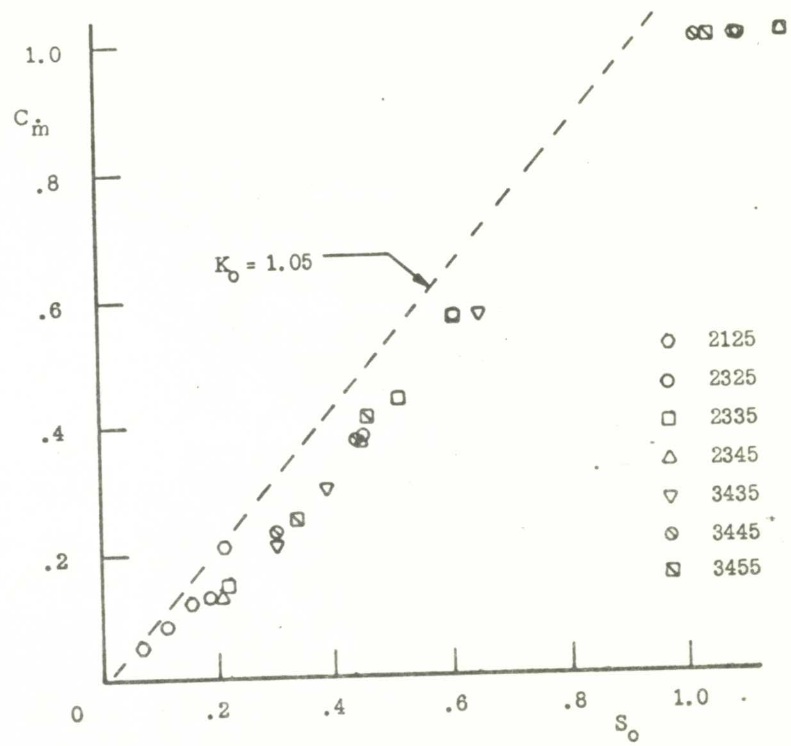

Plenum Vent Shaft With Outflow

FIGURE (24)

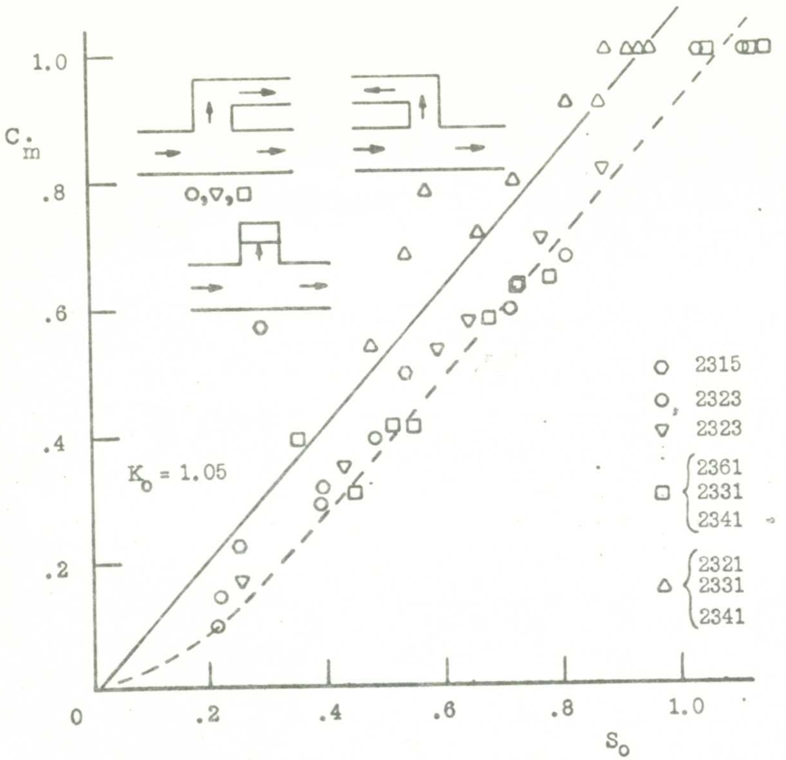

Miter Vent Shaft With Outflow

FIGURE (25)

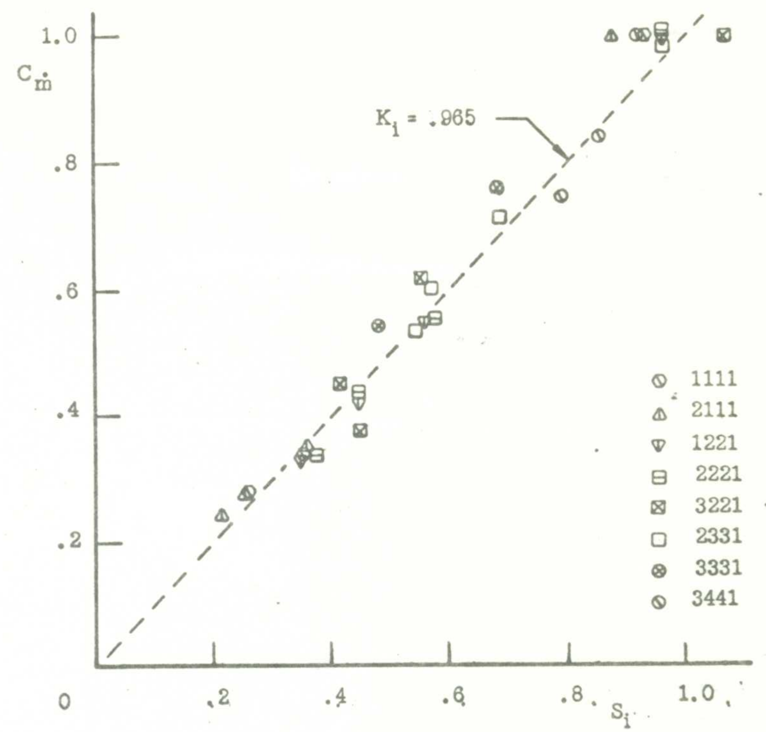

Straight Vent Shafts With Inflow

$C_{\Delta P_S} = 1.0$

FIGURE (26)

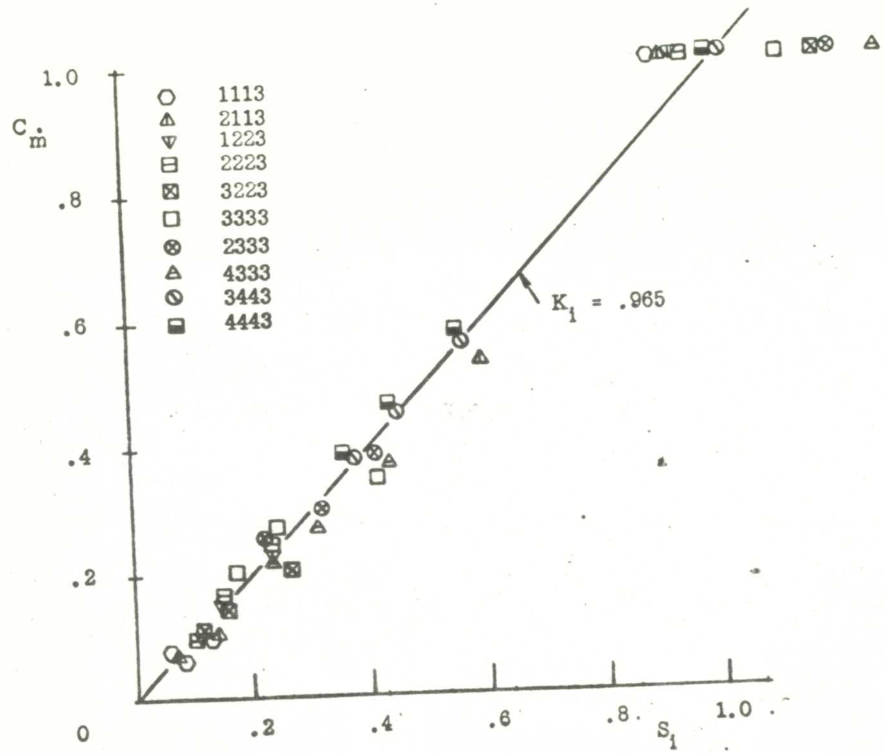

Straight Vent Shafts With Inflow

$C_{\Delta p_s} = 6.5$

FIGURE (27)

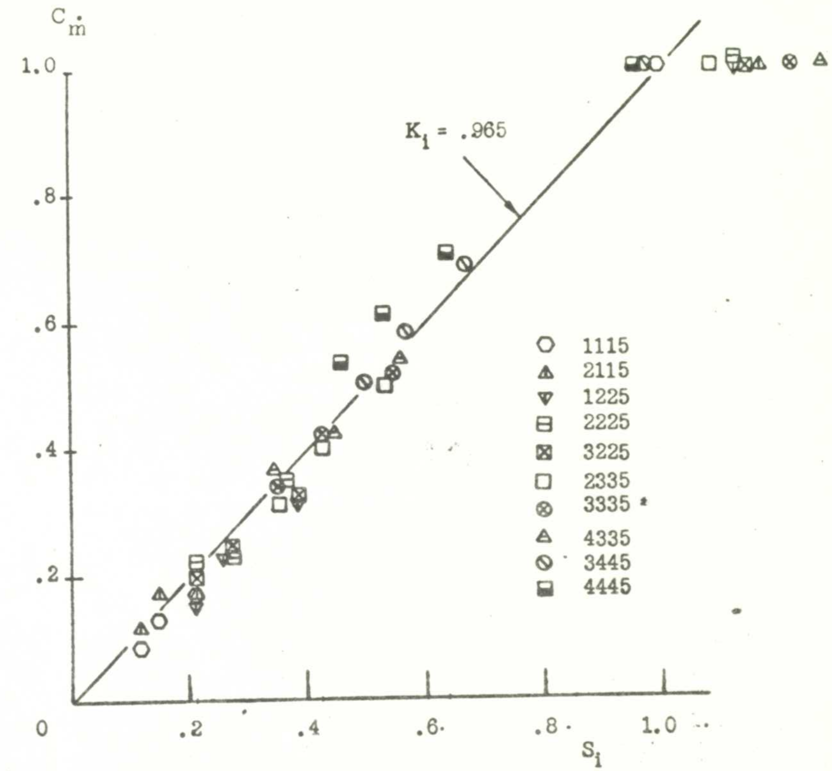

Straight Vent Shafts With Inflow

$C_{\Delta p_s} = 17.0$

FIGURE (28)

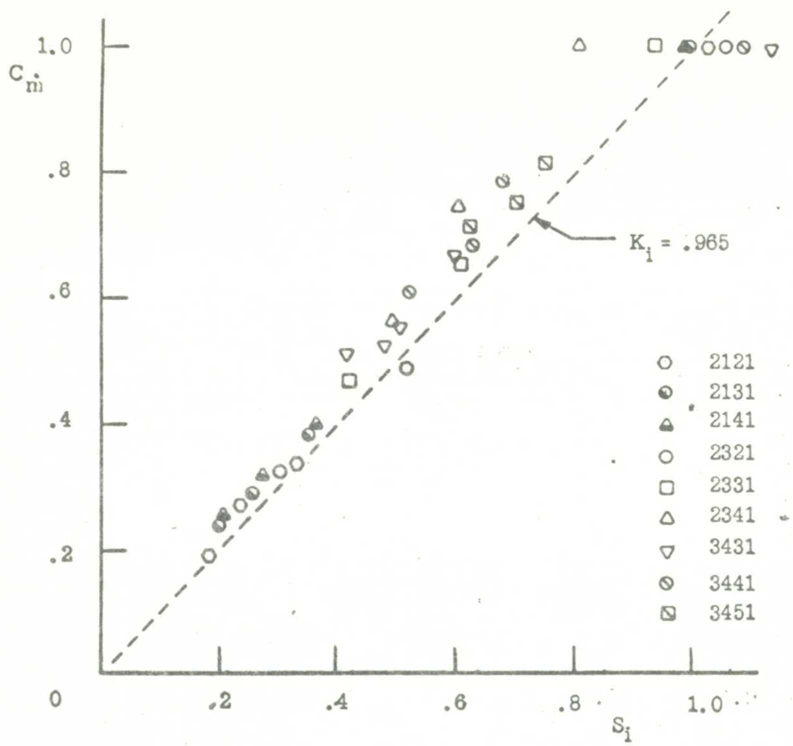

Plenum Vent Shafts With Inflow
For $C_{\Delta p_S}$ see Appendix B
FIGURE (29)

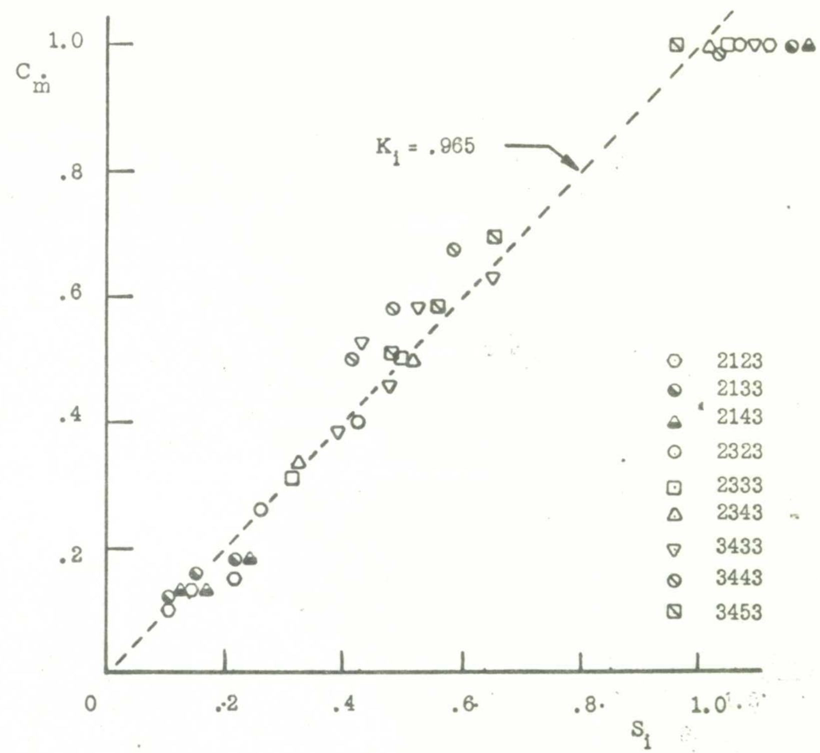

Plenum Vent Shafts With Inflow
For $C_{\Delta p_S}$ see Appendix B
FIGURE (30)

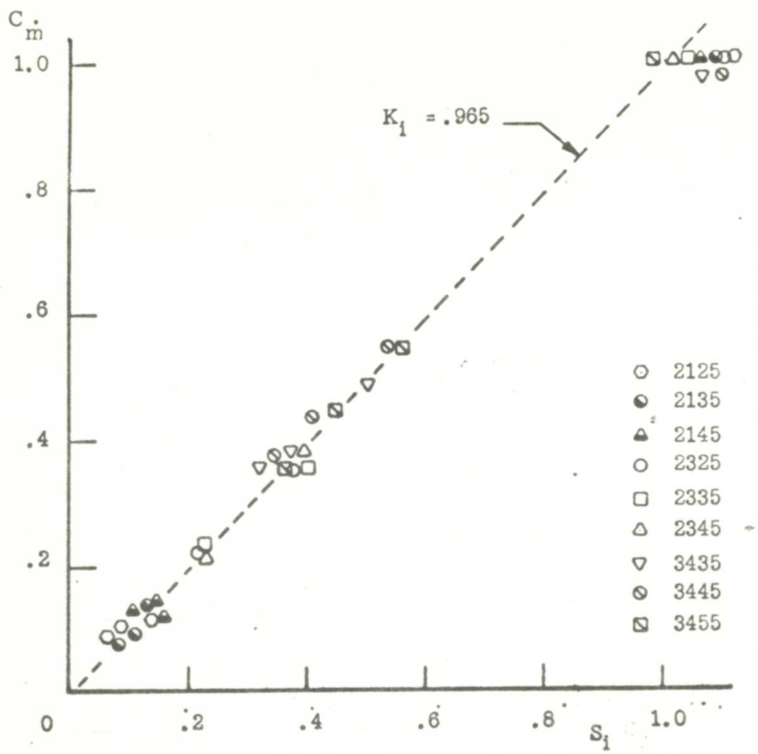

Plenum Vent Shafts With Inflow
For $C_{\Delta ps}$ see Appendix B
FIGURE (31)

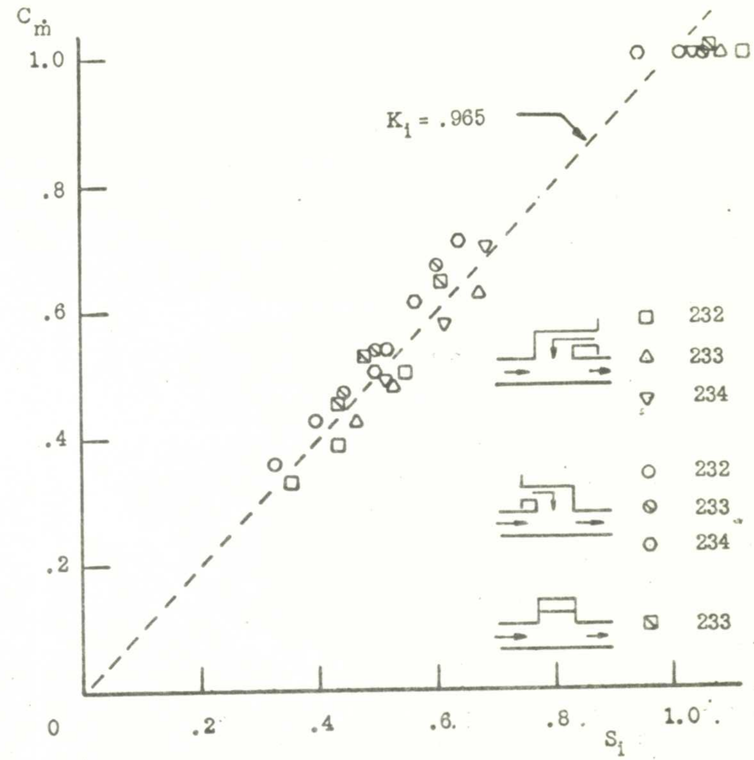

Miter Turn Vent Shaft With Inflow

FIGURE (32)

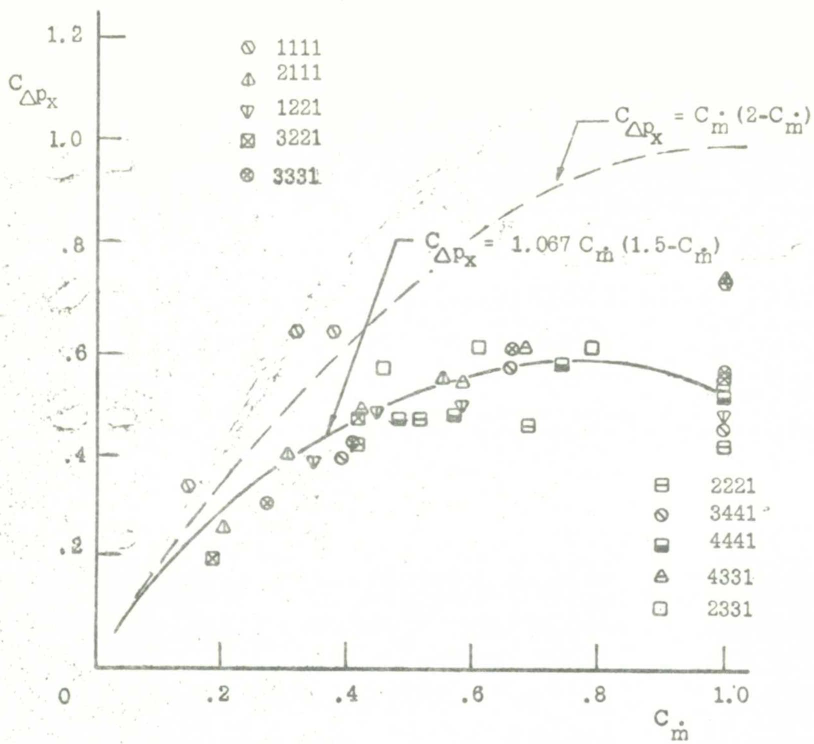

Static Pressure Rise Across Straight Vent Shaft

(Outflow)

$C_{\Delta p_s} = 1.0$

FIGURE (33)

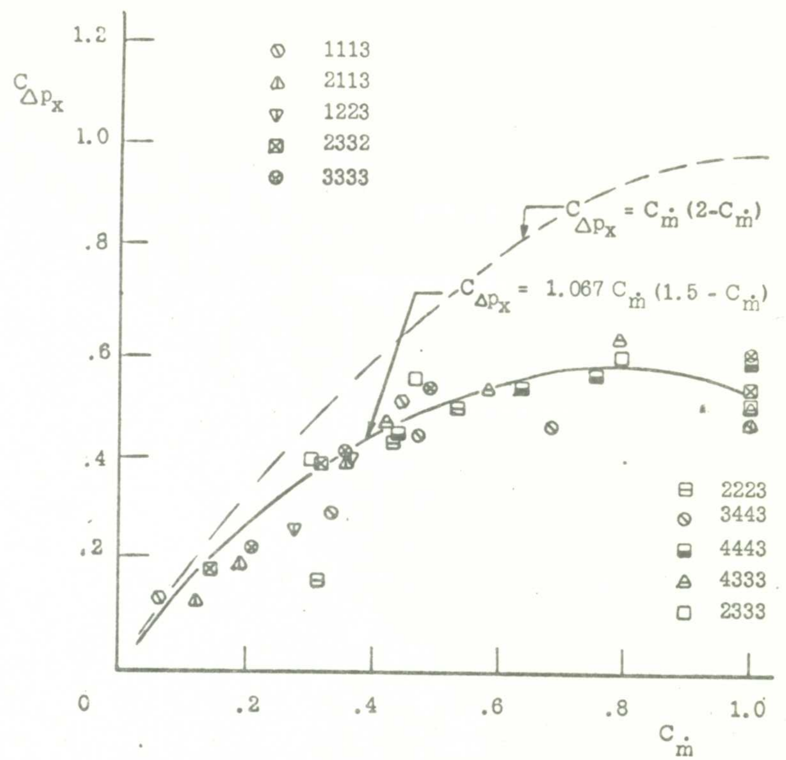

Static Pressure Rise Across Straight Vent Shaft

(Outflow)

$C_{\Delta p_s} = 6.5$

FIGURE (34)

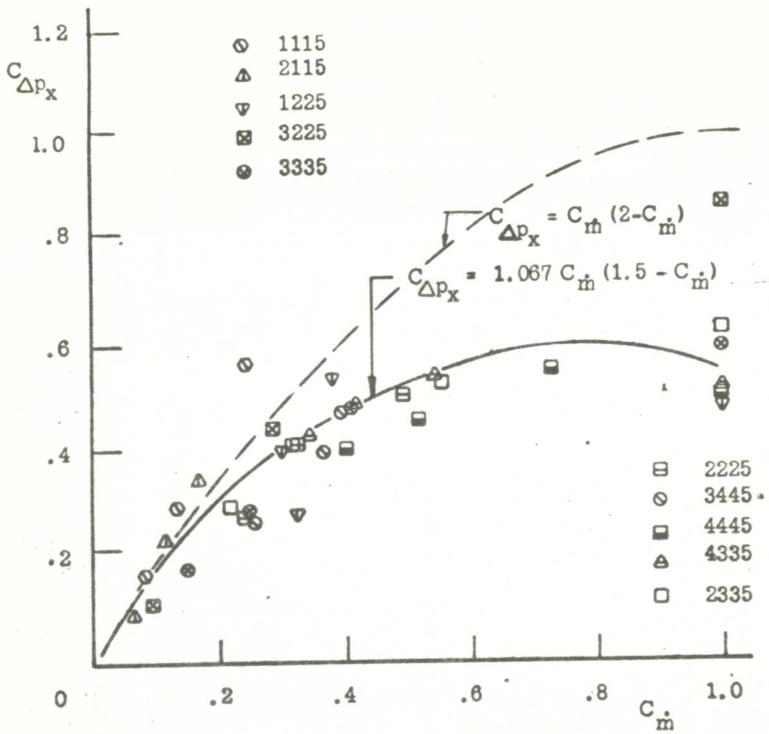

Static Pressure Rise Across Straight Vent Shaft

(Outflow)

$C_{\Delta p_s} = 17.0$

FIGURE (35)

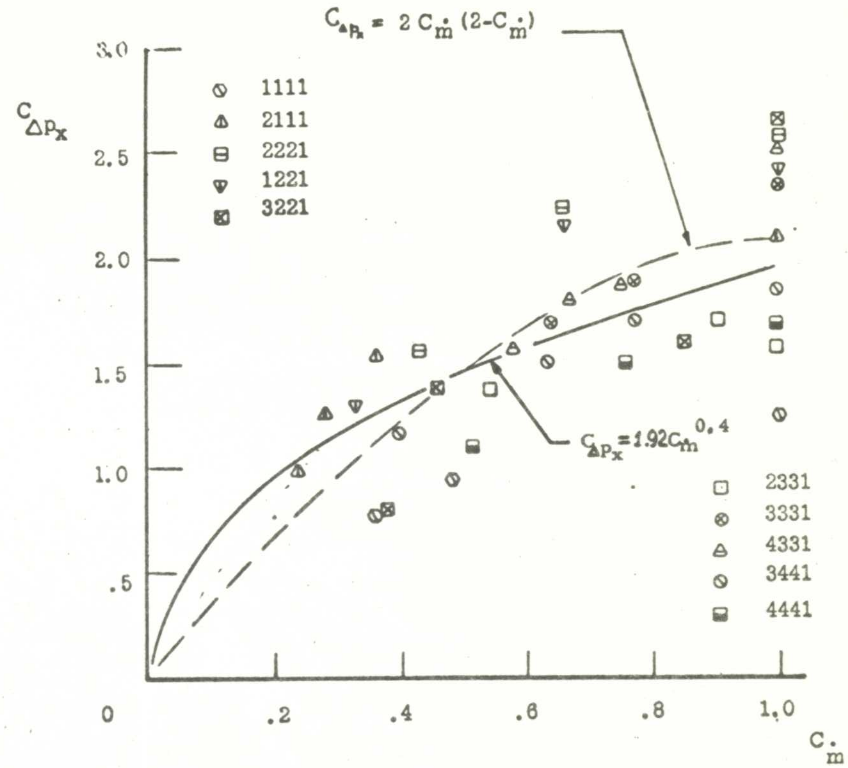

Static Pressure Drop Across Straight Vent Shafts With Inflow

$C_{\Delta p_s} = 1.0$

FIGURE (36)

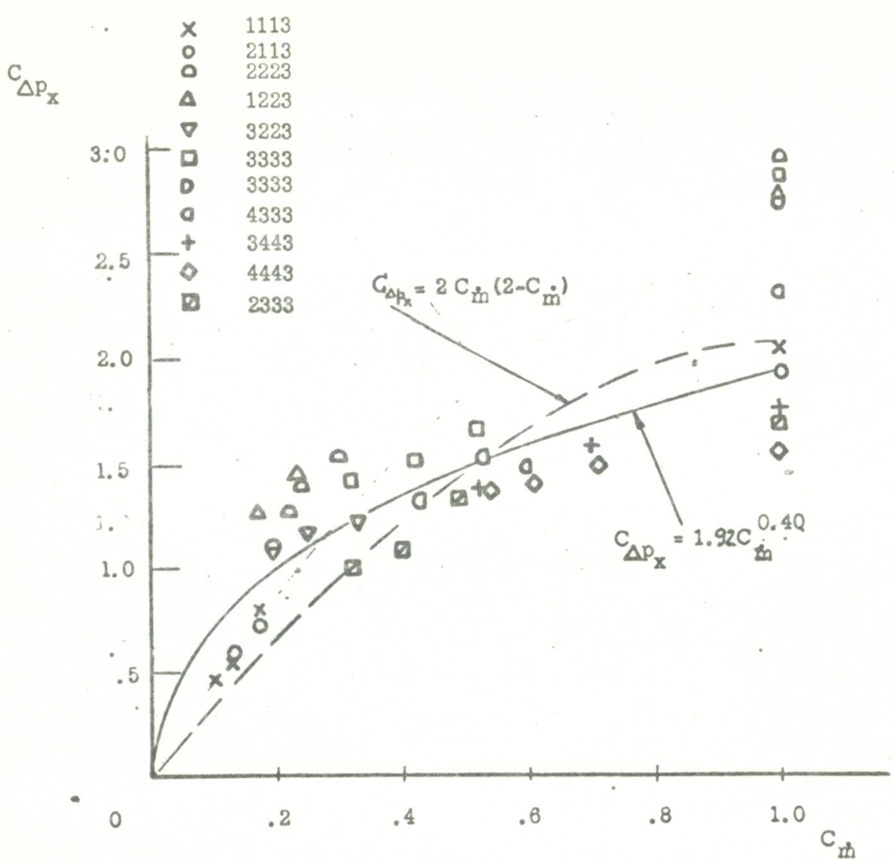

Static Pressure Drop Across Straight Vent Shaft Inflow

$C_{\Delta p_x} = 6.5$

FIGURE (37)

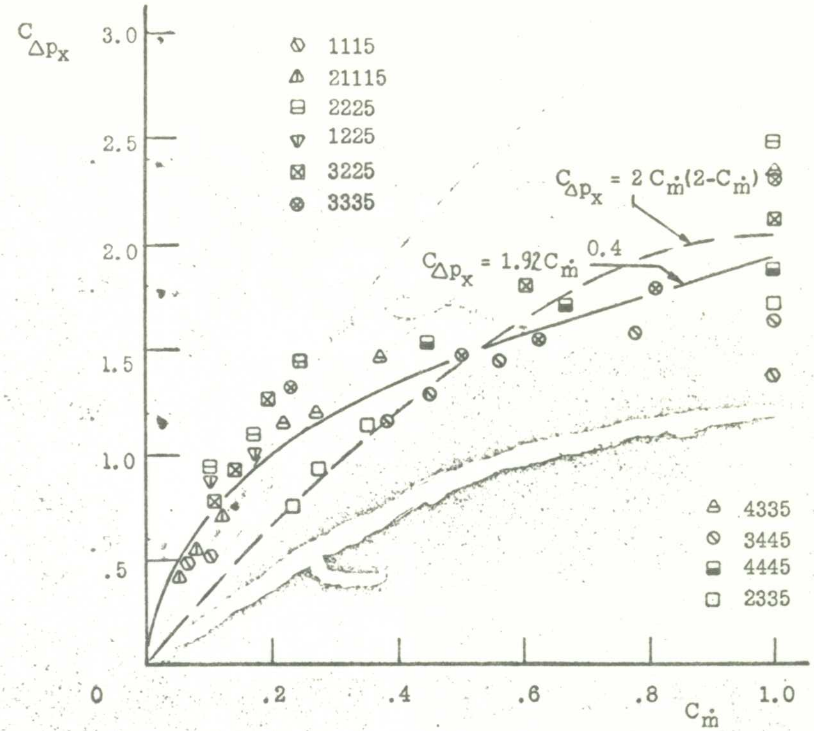

Static Pressure Drop Across Straight Vent Shaft (Inflow)

$C_{\Delta p_s} = 17.0$

FIGURE (38)

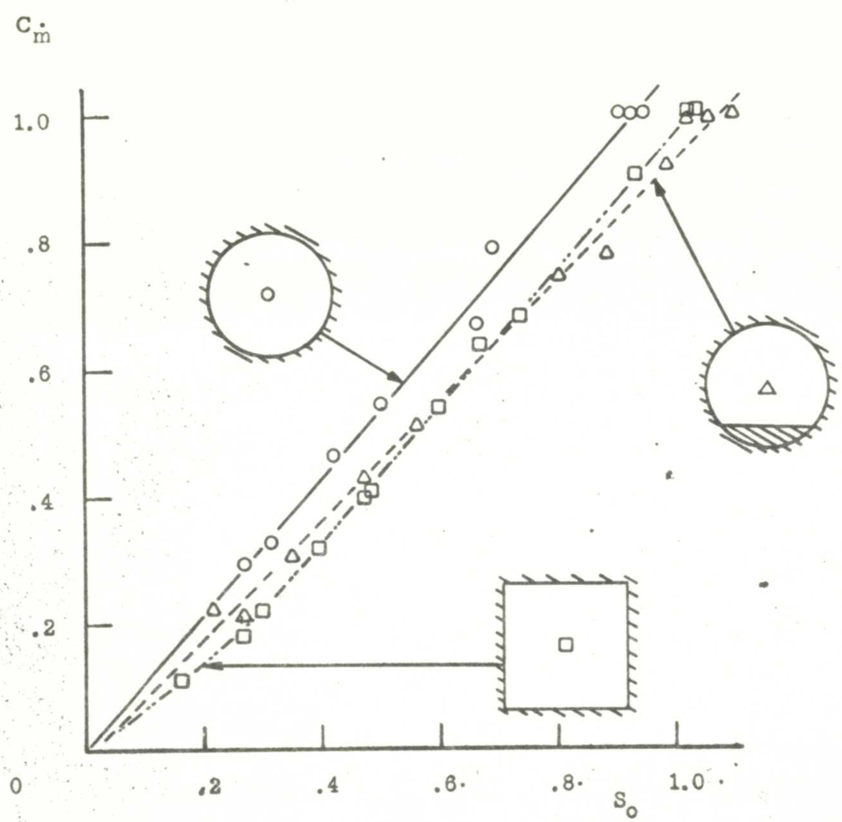

Effect of Tunnel Cross-Section
(Outflow)
$C_{\Delta p_s}$ Values
$0 < C_{\Delta p_s} < 23$
FIGURE (39)

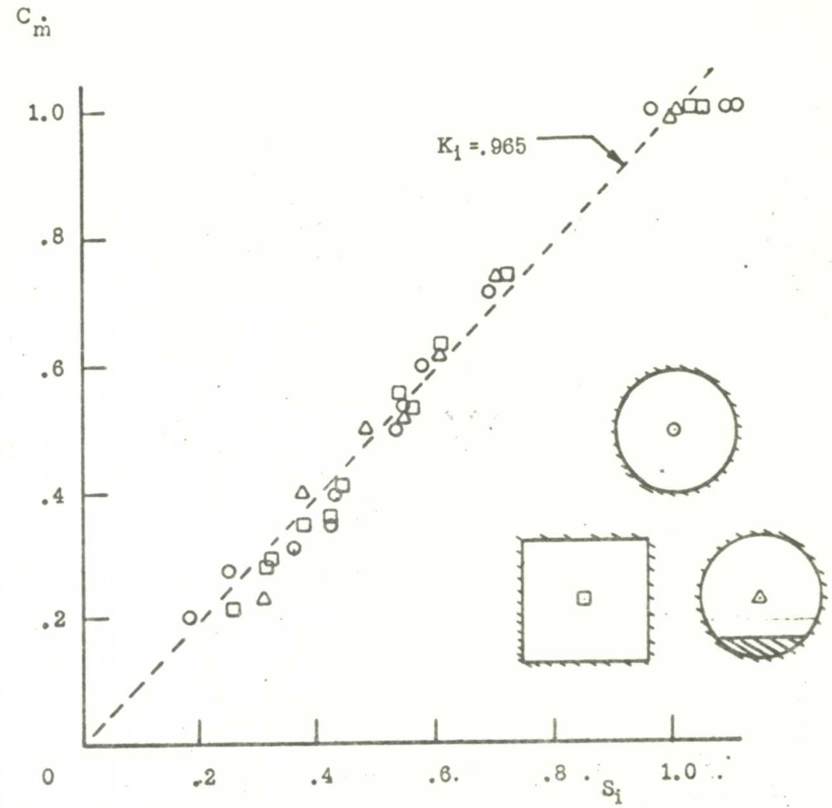

Effect of Tunnel Cross-Section
(Inflow)
$C_{\Delta p_s}$ Values
$0 < C_{\Delta p_s} < 23$
FIGURE (40)

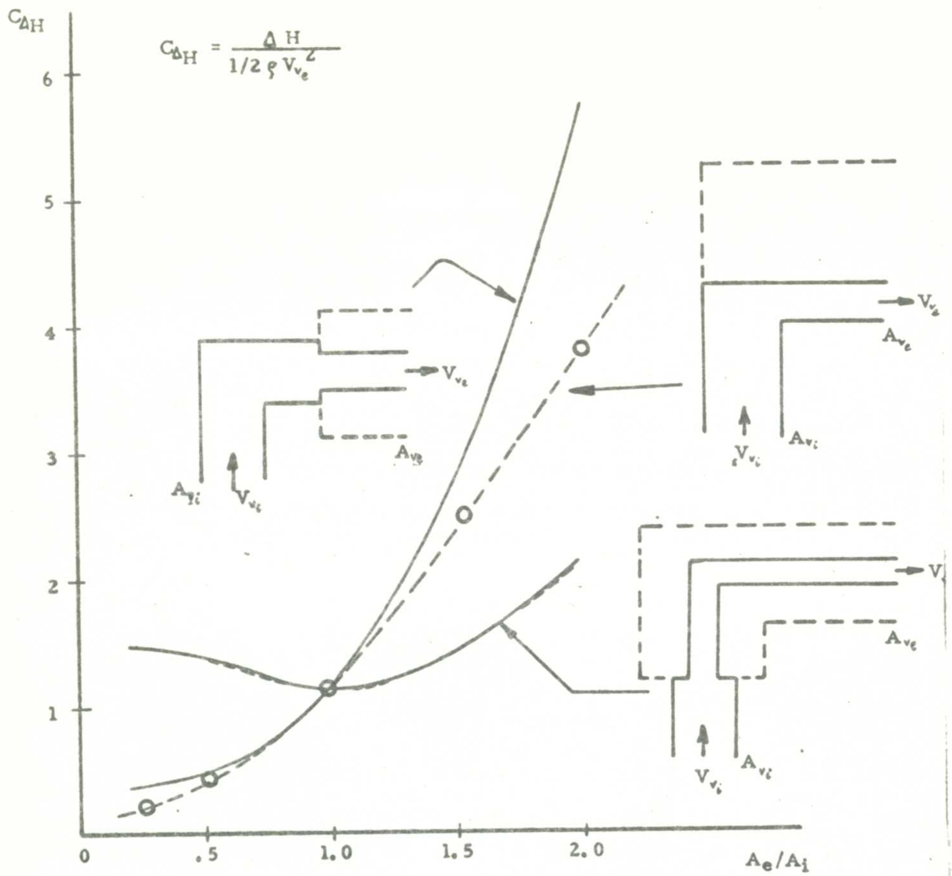

Losses In Contracting and Expanding Miter Turns

FIGURE (41)

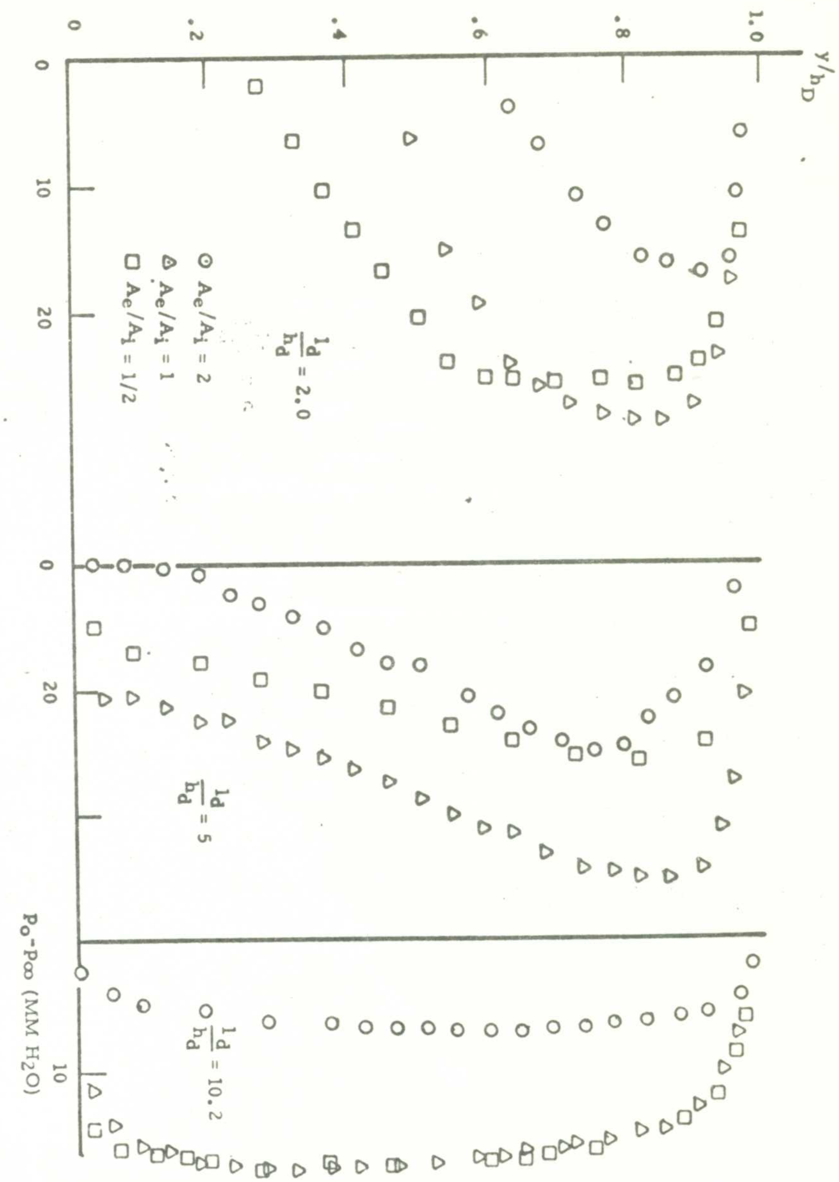

Total Head Distribution Across Miter Mixing Duct

FIGURE (42)

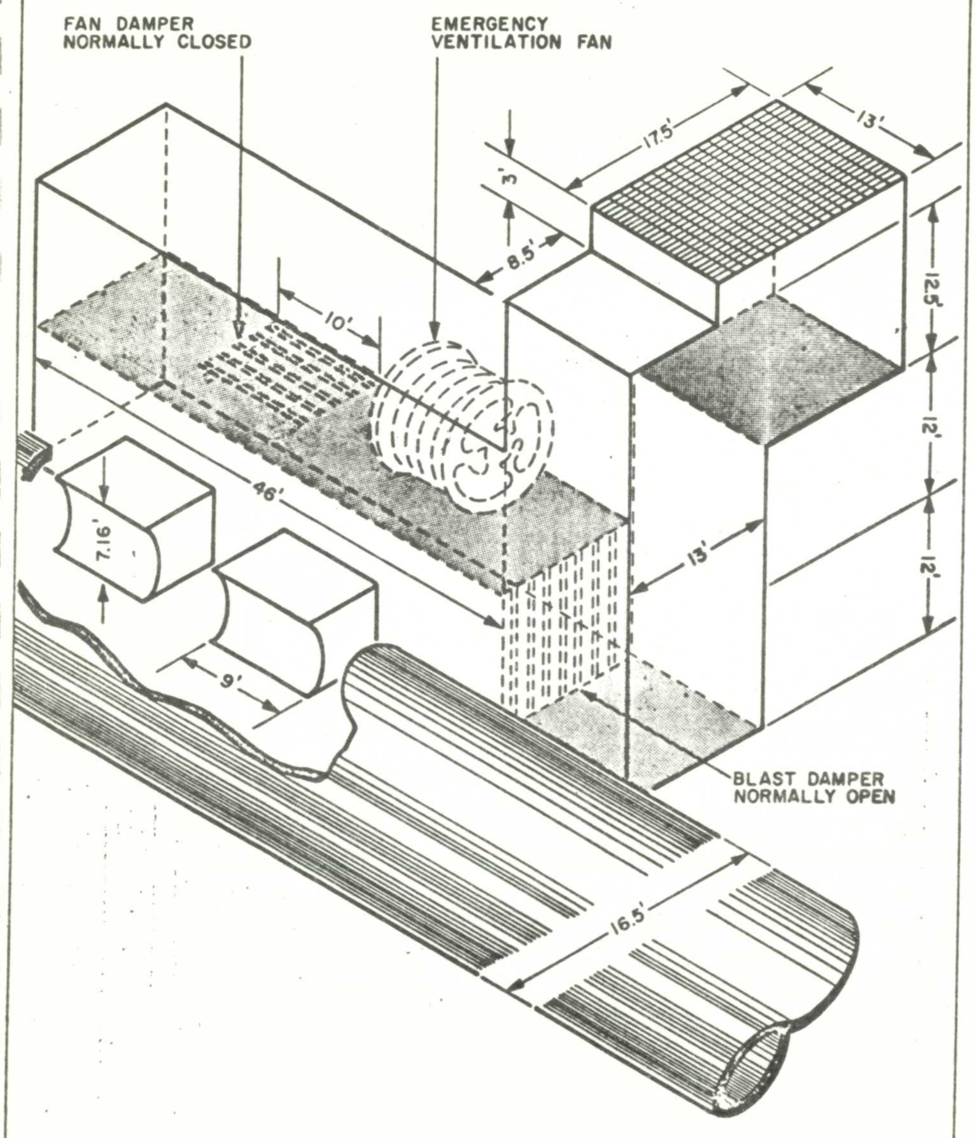

FIGURE (43)
BART, TWO-PORT RECTANGULAR INLET SECTION

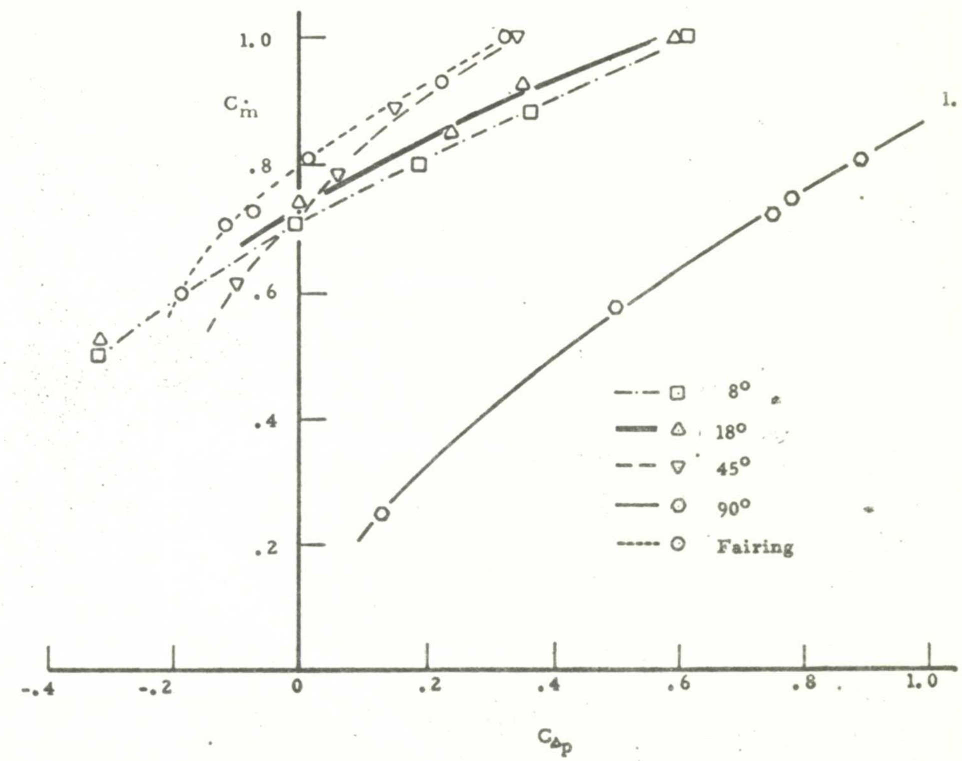

Variable Inlet - Outflow

$C_{\Delta p_s} = 1.0$

FIGURE (44)

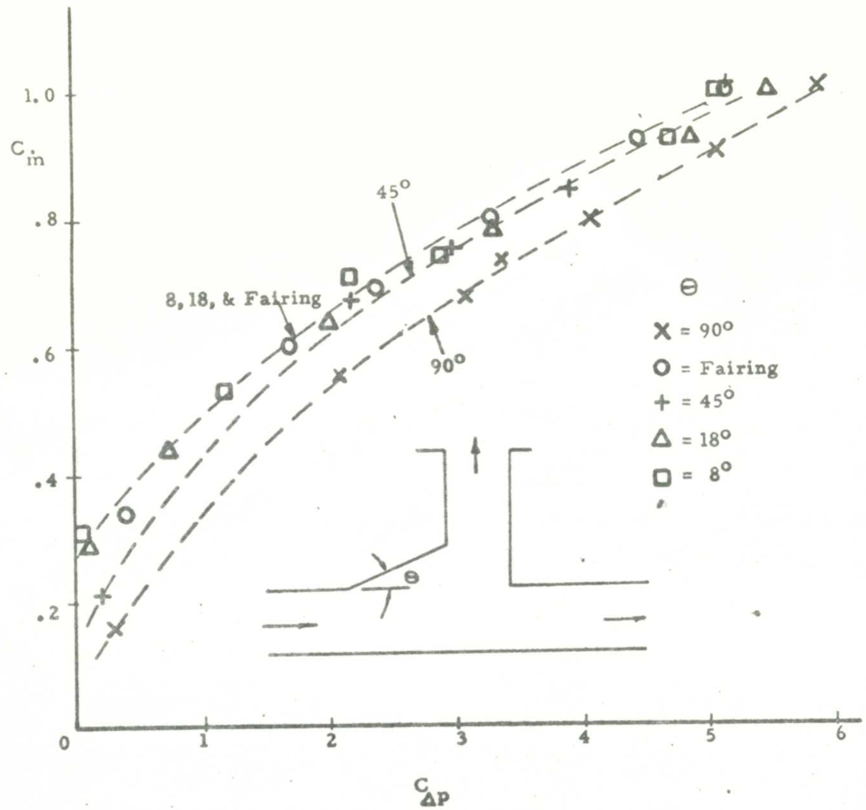

Variable Inlet - Outflow

$C_{\Delta p_s} = 6.5$

FIGURE (45)

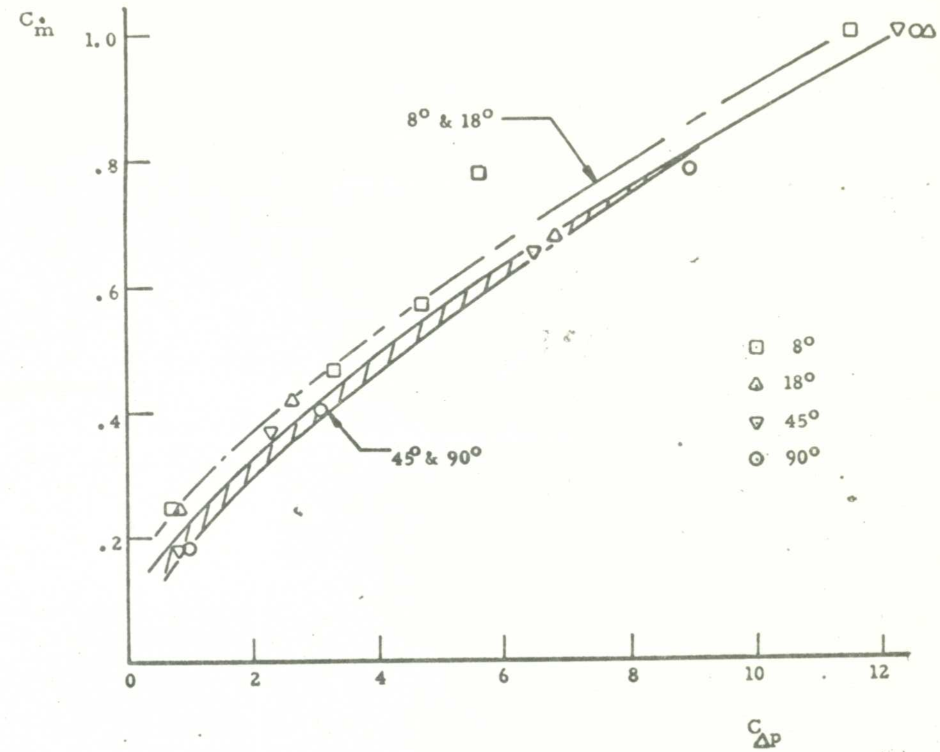

Variable Inlet - Outflow

$C_{\Delta p_s} = 17$

FIGURE (46)

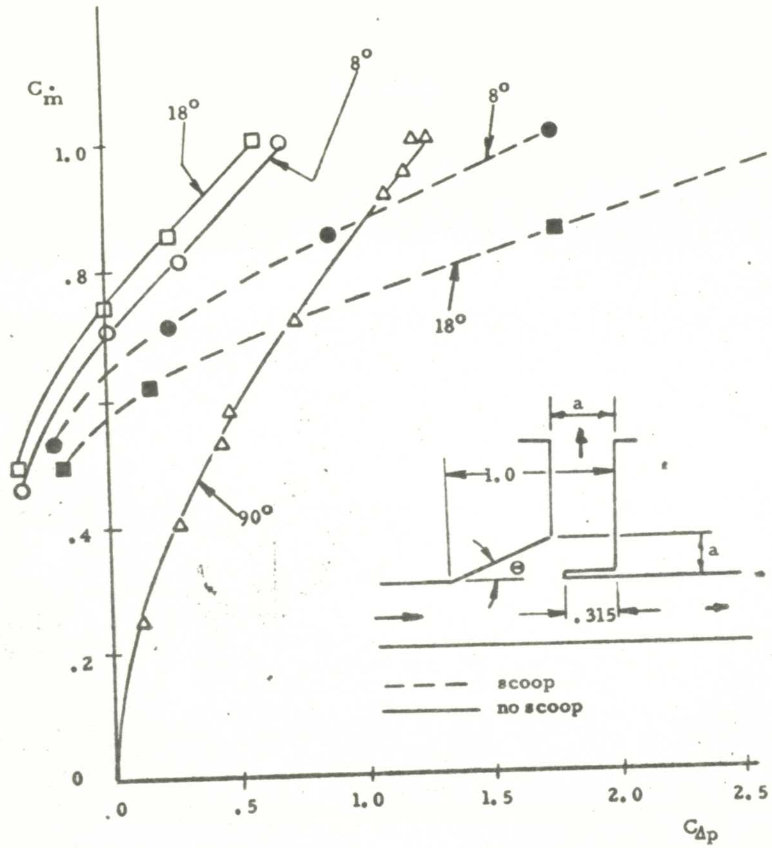

Effect of Scoop With Outflow

$C_{\Delta p_s} = 1.0$

FIGURE (47)

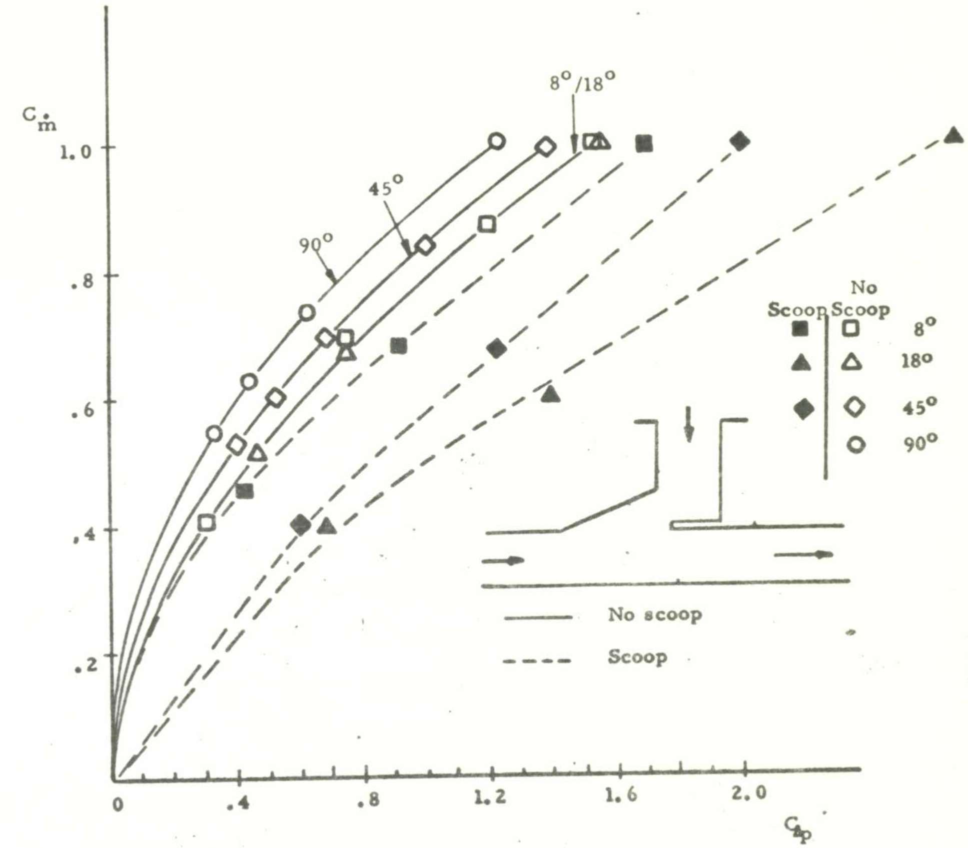

Variable Inlet With Inflow

Scoop & No Scoop

$C_{\Delta p_s} = 1.35$

FIGURE (48)

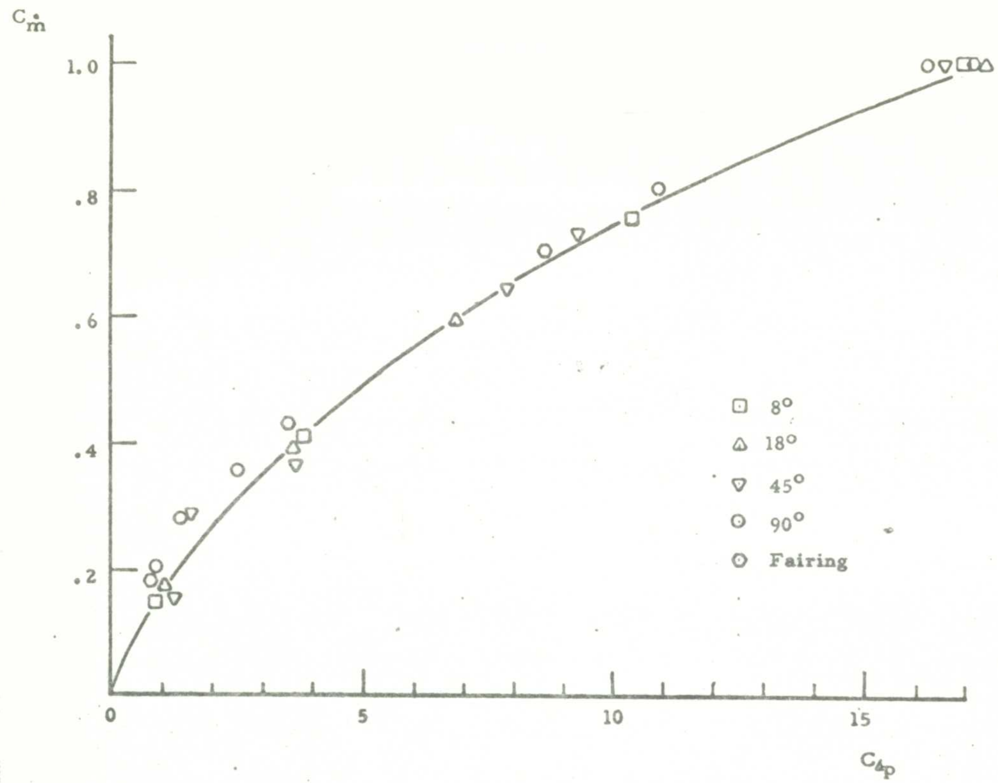

Variable Inlet With Inflow

$C_{\Delta p_s} = 16.2$

FIGURE (49)

APPENDIX A

DSI-AT VENT SHAFT & STATION (VST)
TEST FACILITY

A.1 VST FACILITY OPERATION & PROCEDURES

The general configuration of the VST facility is depicted schematically in Figure (1). It consists of a plenum box 4'x5'x6' supplied with air at 1.75 psig at a volume flow rate up to 4800 cfm. Air flows through a cooling coil into the plenum box then into a 12" i.d. tube (same tube used in moving vehicle test facility) in which the mass flow rate is measured by means of a DISA hot wire mass-flow meter ($\dot{m}_1$) or integrating pressure rake. A tube length of 20 diameters is provided downstream of the inlet to permit a fully turbulent flow profile to be developed.

At the downstream end of the rig is the ETL (effective tunnel loss) valve assembly which can be accurately adjusted to simulate pressure drops corresponding to exit tube length/diameter ratios between 0 and ∞. The ETL valve assembly is mounted on a carriage so that it can be displaced axially to accommodate test sections varying between 0 and 50'. Just upstream of the ETL valve is another DISA mass-flow anemometer ($\dot{m}_2$) or integrating rake.

For suction, the blower valves are changed and flow enters a 20 foot tube through an inlet fairing to permit fully developed turbulent flow. It then passes the test section and through the plenum box, and is exhausted by the blowers. Mass flow rate is measured before the test section and again before the plenum box. Screens are used after the test section to allow the flow to fully develop before the mass flow measurements are taken.

The plenum box is used directly with the vent shaft to exclude the vent inlet losses. The vent shaft is attached to a transition box on the top of the

plenum, and for blowing a 17 $^1/_2$ inch diameter tube with an inlet fairing and screens are used to measure the mass flow rate. For suction a 7 $^1/_2$" nozzle is used for mass flow measurements.

A schematic representation of the VST facility is shown in Figure (1). A sound proofing box is placed around the blowers and special material is also used inside the plenum to attenuate the sound reverburations.

Figure (2) shows the vent shaft setup for blowing on the plenum. The transition section has faired inlet that provides the vent shaft with an ideal loss free inlet.

Figure (3) shows the vent shaft setup for suction. A ground plane is added at the tope of the vent shaft to simulate the pavement or ground level. A screen is used inside the transition section to provide uniform flow into the nozzle for mass flow measurement.

Figure (4) shows the control vent shaft setup "in situ". The location for suction and blowing mass flow rate measurements are shown in the figure.

Figure (5) shows the miter vent shaft in both the plenum setup and "in situ".

Figure (6) shows the variable inlet vent shaft "in situ". For suction the vent shaft section was turned 180° around.

Figure (7) shows the SAT vent shaft "in situ".

A.2 INSTRUMENTATION

The following is the list of instrumentations used for the vent shaft testing.

ITEM NO.	DESCRIPTION	FUNCTION
1.	Multi-manometer	To define the static pressure at different locations in the vent shaft.
2.	Micro-manometer & pitot tube or integrating rake.	To measure air velocity.
3.	Hot wire anemometer	To measure air velocity in the tube and vent shaft.
4.	Pressure transducer	To measure the static pressure of plenum chamber.
5.	Standard Barometer	To measure the local atmospheric pressure.
6.	Thermocouples	To measure atmospheric and plenum chamber temperature.
7.	Digital Voltmeter	To read the output of the anemometer.
8.	Traversing Mechanism	To traverse with the anemometer.
9.	X-Y Plotter	To plot velocity vs position of the anemometer.

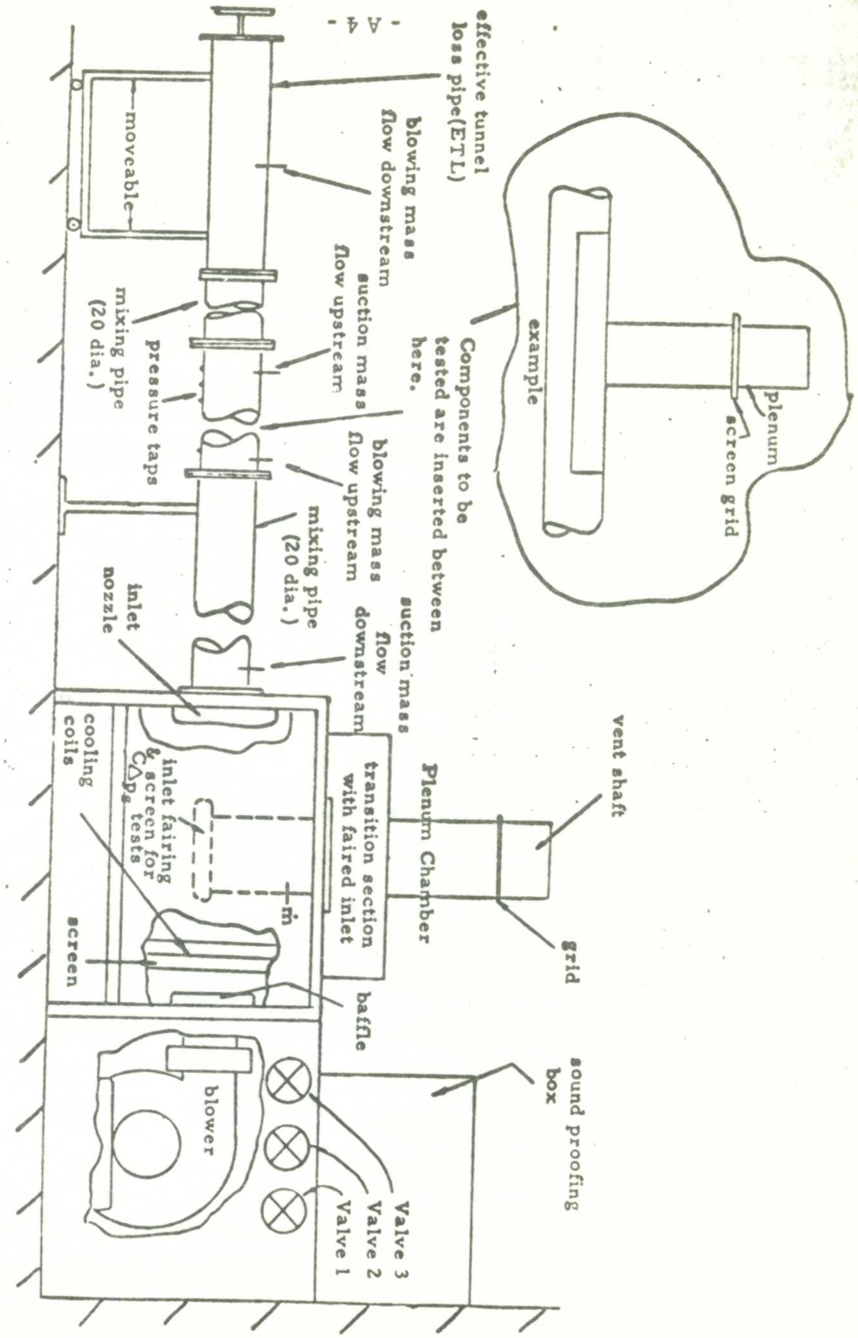

FIGURE A-1

Schematic Representation of the VST Facility

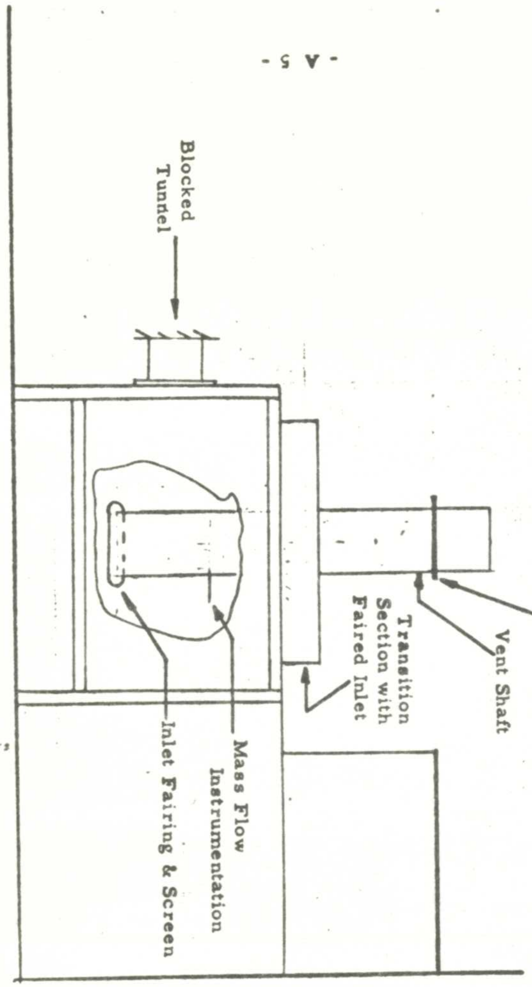

FIGURE (A-2) Vent Shaft Setup for Blowing on Plenum

APPENDIX B

CONTROL VENT SHAFT CODE SYSTEM

The control vent shaft test parameters are defined as follows:

Aspect ratio	Refers to the inlet opening of the vent shaft. The length of the inlet parallel to the tunnel (b) divided by the width of the opening, $^b/_w$.
Inlet area ratio	The inlet area of the vent shaft (A_{v_i}) divided by the tunnel area (A_t).
Exit area ratio	The exit area of the vent shaft (A_{v_e}) divided by the tunnel area (A_t).
Vent Shaft Loss Coefficient (impedance)	The total loss coefficient $C_{\Delta p_s}$ thru the vent shaft from the plenum box to atmosphere where the inlet conditions are ideal.

The code system that was used consists of four digits in the following order:

I.	First digit	Signifies Aspect ratio
II.	Second digit	Signifies Inlet Area ratio
III.	Third digit	Signifies Exit Area ratio
IV.	Fourth digit	Signifies Shaft Loss Coefficient

The range of each variable and the appropriate codes are listed below:

Code I = Aspect ratio = $^b/_w$

1 = 0.5
2 = 1.0
3 = 5.0
4 = 10.0

Code II = Inlet Area/Tunnel Area = $\frac{A_{v_i}}{A}$

1 = 0.25
2 = 0.5
3 = 1.0
4 = 2.0

Code III = *Exit Area/Tunnel Area = $\frac{A_{v_e}}{A}$
(Using an exit plenum box attached to the vent shaft exit)

1 = 0.25
2 = 0.5
3 = 1.0
4 = 2.0
5 = 5.0

Code IV = Vent Shaft Loss Coefficient
(Using different mesh grids in the vent shaft)

1 = Low impedance
3 = Medium impedance
5 = High impedance

Table I below lists the actual impedance values for each vent shaft. For blowing the values were identical for all straight vent shafts (i.e., without the exit plenum box).

---

*For the miter vent shaft 6 = 1.5

VENT SHAFT IMPEDANCE VALUES

Vent Code			Impedance IV					
			Blowing			Suction		
I	II	III	1	3	5	1	3	5
1	1	1	1.0	6.5	17	1.4	6.0	16
2	1	1	1.0	6.5	17	1.34	5.48	16
1	2	2	1.0	6.5	17	1.4	5.97	16
2	2	3	1.0	6.5	17	1.31	5.61	16
3	2	2	1.0	6.5	17	1.4	5.73	16
2	3	3	1.0	6.5	17	1.3	6.0	16.2
3	3	3	1.0	6.5	17	1.38	6.34	16.5
4	3	3	1.0	6.5	17	1.42	5.94	16.5
3	4	4	1.0	6.5	17	1.2	6.5	18
4	4	4	1.0	6.5	17	1.7	7.0	18.6
With Plenum Chambers								
2	1	2	5.3	18	25	1.72	6.15	16
2	1	3	3.7	16.5	24	1.34	5.63	16
2	1	4	3.3	17	32	1.22	5.64	16
2	3	2	5.3	18	25	7.29	11.9	20.8
2	3	3	1.9	6.2	16.5	2.34	7.05	16.7
2	3	4	1.2	5.5	15	1.28	6.11	15.7

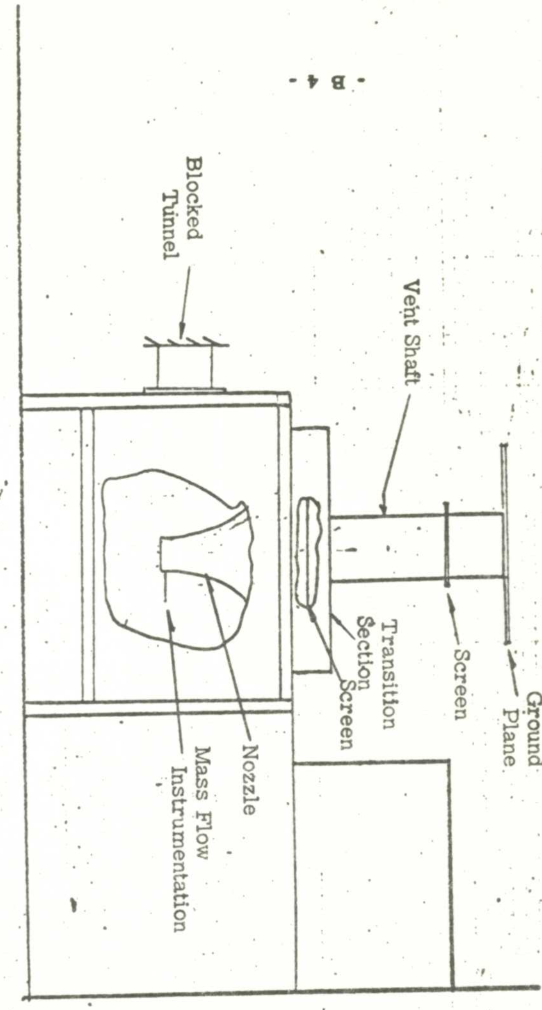

FIGURE (B-1) Vent Shaft Setup for Suction on Plenum

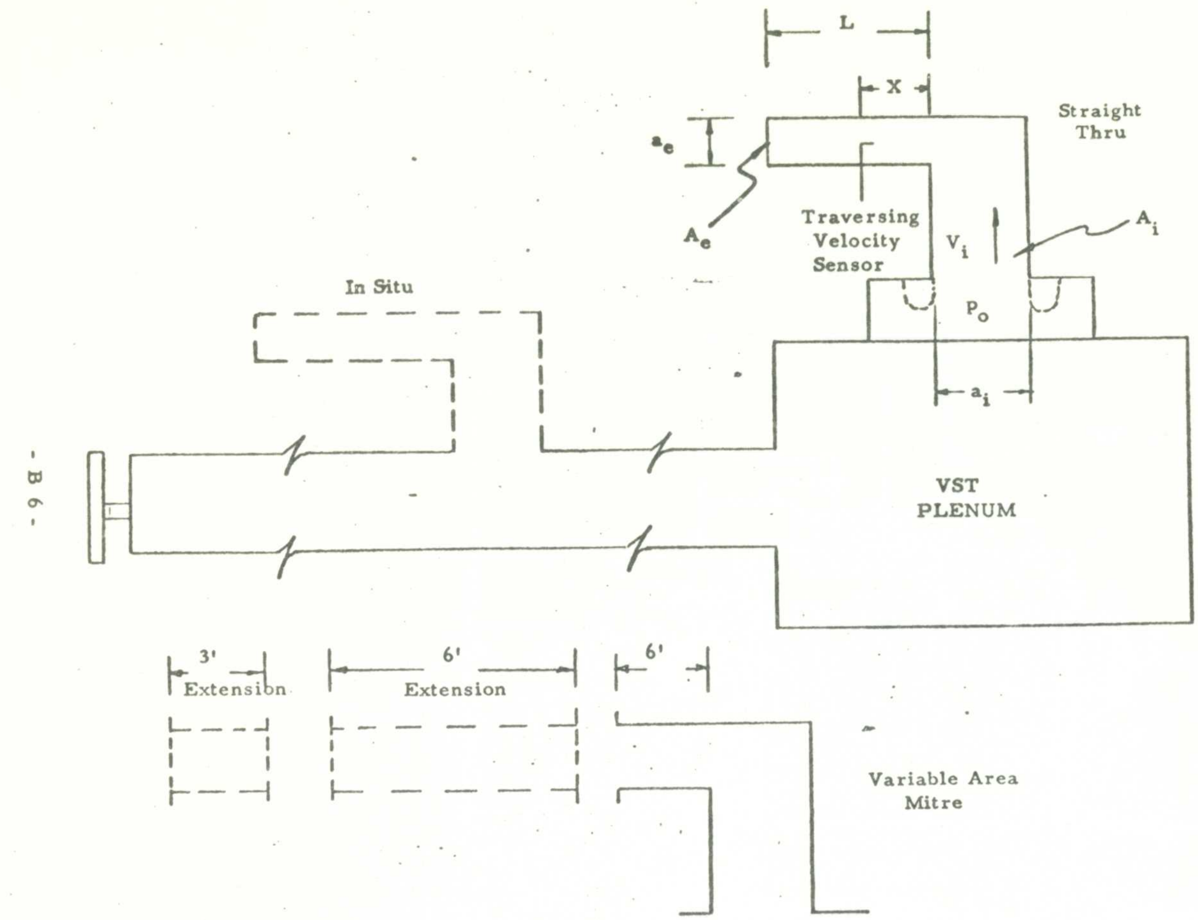

FIGURE (B - 3) SCHEMATIC OF TEST SET UP

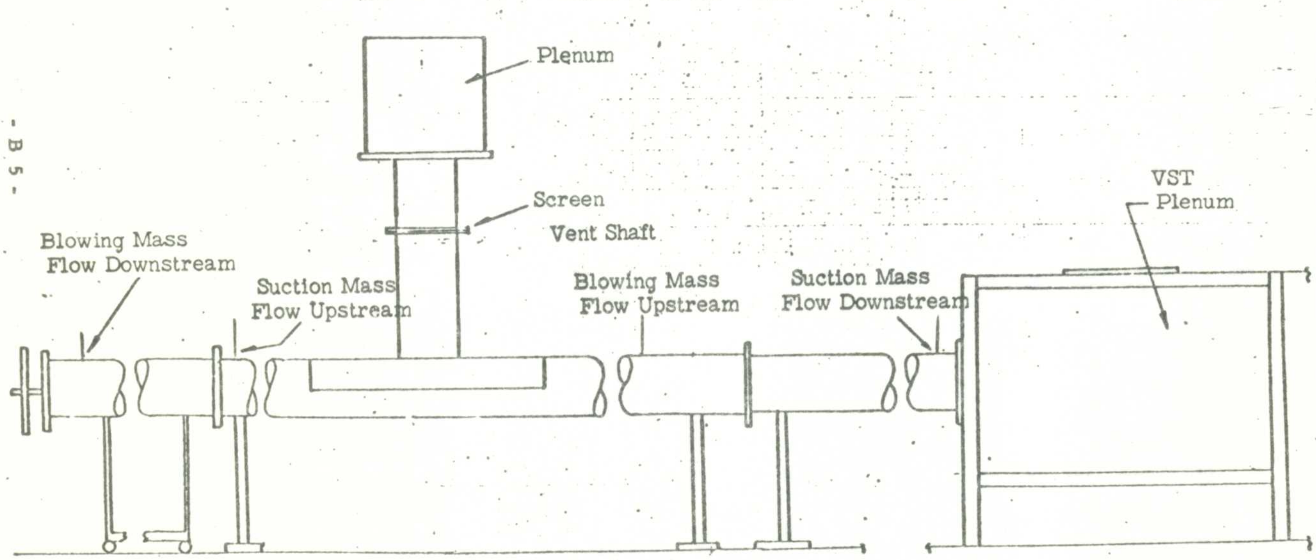

FIGURE (B-2) Control Vent Shaft Test Setup in tunnel

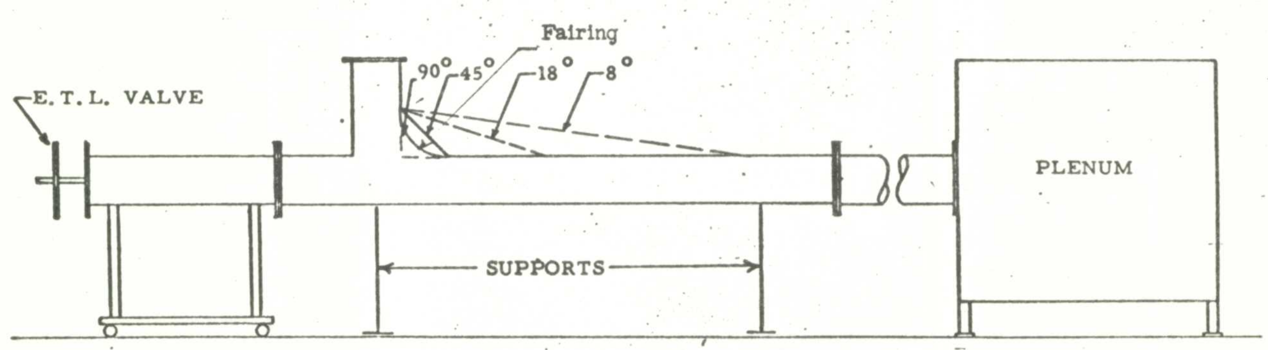

VARIABLE INLET VENT SHAFT
FIGURE (B - 4)

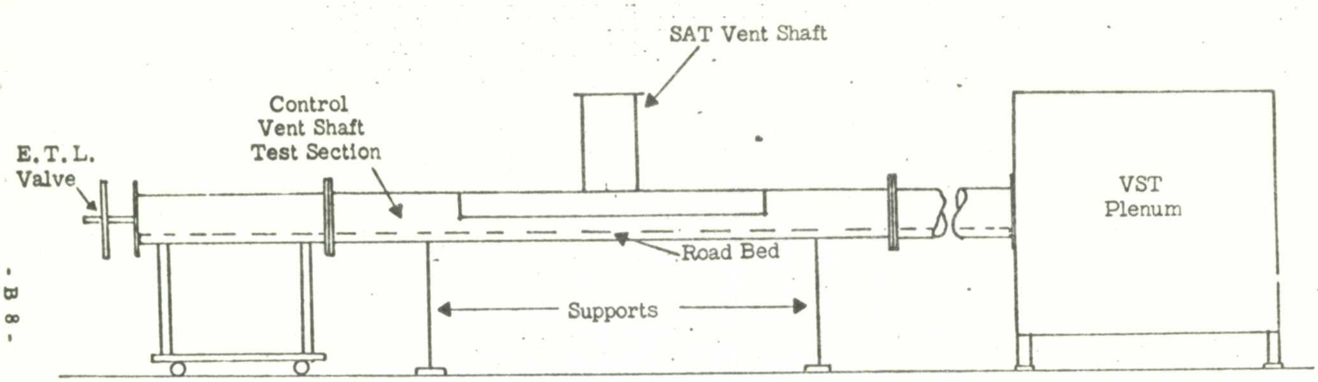

SAT VENT SHAFT SET-UP
FIGURE (B - 5)

VENT SHAFT IMPEDANCE VALUES

Vent Code			Impedance IV Blowing			Suction		
I	II	III	1	3	5	1	3	5
With Plenum Chambers (continued)								
3	4	3	7.9	12.5	22.5	8.5	15.52	27
3	4	4	2.3	7.7	18	3.17	8.63	14.88
3	4	5	1.3	6.0	16.5	1.4	6.8	18.6
Miter Vent Shaft								
2	3	1	21	N/A	N/A			
2	3	2	7.0	"	"		5.85	
2	3	6	1.7	"	"			
2	3	3	2.5	"	"		2.44	
2	3	4	1.2	"	"		1.55	
2	3	2	7.0	"	"			
2	3	3	2.5	"	"		2.44	
2	3	4	1.2	"	"		6.18	
SAT Vent								
2	3	3	1.4	6.5	N/A	1.2	8.0	N/A
With Exit Area Change								
2	3	2	7.0	19.0		4.0	21	
Variable Inlet Vent (mates with square tunnel)								
2	3	3	1.0	6.5	17	1.35	5.65	16.2

Examples of using the code system:

A. 1 2 2 5
a b c d

- a. Aspect ratio = 0.5
- b. Inlet Area ratio = 0.5
- c. Exit Area ratio = 0.5
- d. Loss Coefficient (Table I) = 17.0 Blowing or 16 Suction

B. 2 3 4 3 (Exit Plenum Box)
a b c d

- a. Aspect ratio = 1.0
- b. Inlet Area ratio = 1.0
- c. Exit Area ratio = 2.0
- d. Loss Coefficient = 5.5 Blowing or 6.11 Suction

APPENDIX C
ERROR ANALYSIS

An analysis was performed to find the influence of the error band of the raw data on the final reduced parameters.

Two cases are presented. The first of a small vent shaft where the mass flow rate is low and the pressure values are also low. The second is for the medium and larger area vent shafts which constituted 85% of all vents tested.

The error band for the water manometers that are used to measure upstream and downstream pressures is $\pm$ 0.05 inches. Their maximum useful range is 36". To measure velocity a delta micromanometer was used with an accuracy of $\pm$ 2.5 mm on the most sensitive reading range (.05 x scale).

A limitation on the small vent shafts with large values of $C_{\dot{m}}$ was the maximum static pressure that could be read without blowing the water manometers. That being 34 inches of water occuring at high $C_{\dot{m}}$ ($\simeq 1$). As a worst case example using a vent shaft with an inlet area of 1/4 that of the tunnel area and a high vent impedance, (i.e. 17);

$$C_{\dot{m}} = \frac{A_{v_i}}{A} \sqrt{\frac{C_{\Delta p}}{C_{\Delta p_s}}}$$

or $$C_{\Delta p} = \left(\frac{A}{A_{v_i}}\right)^2 C_{\Delta p_s} \quad \text{when } C_{\dot{m}} = 1$$

therefore $$C_{\Delta p} = 16 \times 17 = \frac{p_1 - p_\infty}{\frac{1}{2}\rho V_1^{\,2}} = \frac{p_1 - p_\infty}{\Delta p_u}$$

Using the maximum travel of the manometers - 34 inches,

$$\Delta p = \frac{p_1 - p_\infty}{(16)(17)} \quad \frac{34}{(16)(17)} = .175 \text{ inches}$$

or equivalent to 87 mm on the .05 scale.

The uncertainty on the measurement of $C_{\dot{m}}$ is

$$C_{\dot{m}} = \frac{\pm 2.5}{87.} = \pm 3\% \; ; \; C_{\dot{m}_V} = \pm 6\%$$

For measuring $C_{\Delta p_x}$ at $C_{\dot{m}} = 1$

From the data

$$C_{\Delta p_x} = \frac{\Delta p_x}{\Delta p_u} = \frac{0.4 \pm .05}{.175} = 2.3 \pm .285$$

or worst error band on $C_{\Delta p_x}$ is:

$$C_{\Delta p_x} = \pm 12\%$$

For case two, representative of approximately 85% of the vent shafts tested, the nominal error for $C_{\Delta p_x}$ from the data is

$$C_{\Delta p_x} = \frac{\Delta p_x}{\Delta p_u} \quad \frac{.9 \pm .05}{7.2}$$

or error of

$$C_{\Delta p_x} = \pm 5.2\%$$

For measurements of $C_{\Delta p_S}$, on top of the plenum box, two micromanometers were used. One was used to measure the mass flow, and the other to measure

the pressure drop across the vent shaft including the $C_{\Delta H_S}$ grids.

For suction, the cross section area where mass flow was measured, was 1/3 the tunnel area. This allowed high manometer reading. Therefore, even on the smallest vent shafts with high $C_{\Delta H_S}$ grids, the accuracy on $C_{\dot{m}}$ was within $\pm$ 5%.

For blowing measurements the mass flow was measured in a section with an area ratio to the tunnel area of 2.0. For small vent shafts and high $C_{\Delta H_S}$ grids, the accuracy was $\pm$ 20%. For the nominal vent shafts (85% of the cases), the accuracy was $\pm$ 7% or better.

The data reduction was performed using a digital computer (IBM 360-67) eliminating any errors in final coefficient computations.